

**CHARACTERIZATION OF MICROPLASTICS IN BOTTLED DRINKING
WATER AND HEAVY METALS IN PLASTIC PACKAGING USING RAMAN
SPECTROSCOPY, LASER INDUCED BREAKDOWN SPECTROSCOPY (LIBS)
AND PRINCIPAL COMPONENT ANALYSIS.**

BRIAN OBARE OSORO

**Research thesis submitted in partial fulfilment of the requirements for the award of
master of science degree in physics of Maasai Mara University.**

2024

DECLARATION AND APPROVAL

DECLARATION

This thesis is my original work and has not been presented for the award of a degree in any university, college or learning institution. In sections where other people's work has been used, citation and acknowledgement have been made.

Candidate: **BRIAN OBARE OSORO**

REG.NO: SM03/JP/MN/13622/2021

Sign Date

APPROVAL

This thesis has been submitted with our approval as University supervisors

Supervisor: **DR.ING. JARED OMBIRO GWARO**

Department of Mathematics and Physical Sciences

Maasai Mara University

Sign Date

Supervisor: **DR. ROBINSON NDEGWA**

Department of Physics

University of Nairobi

Sign Date

DEDICATION

This work is hereby dedicated to my family and friends.

ACKNOWLEDGEMENT

My sincere appreciation goes to my supervisors Dr. Ing. Jared Ombiro Gwaro and Dr. Robinson Ndegwa for the enlightenment and guidance provided during the development of this work. My deepest gratitude goes to Dr. Ing. Jared Gwaro Ombiro for the motivation and financial support to enroll for the master of science (physics) program, a special friend and a mentor who not only believes in me but also always wishes the best for me. I am grateful to Dr. Robinson Ndegwa for the support in the lab work for his clear insights were essential for the success of this work. I appreciate Mr. Omucheni for allowing me to undertake experiments in their lab and assistance offered during data collection stage.

Special thanks to my friends Edmon Thoya and Hezborn Ondieki whom during my visits to Nairobi provided accommodation, company and moral support that was essential for this work. I deeply salute my friends Sankara Aluko, Frankline Wekesa, Abel Saaya, Eliud Yego and Tabitha Alango from whom I have benefited immense encouragement during my stay at Maasai Mara University Physics Lab. I thank my classmates Stephen Okoth, Samuel Muthini and Dorothy Lwambe with whom we began this journey, to you I will be forever indebted for the motivations and company when the journey seemed quite difficult. I appreciate Hannah Moraa and Carolyne Jeptoo of the University of Nairobi for the company and insights at the Laser Lab. I thank Dr. Ombati of the Kenya Bureau of Standards for helping me to procure some samples from Germany during his visit. My gratitude also goes to Prof. Justus Simiyu for constant motivation in ensuring completion of this work.

I sincerely thank my mother, Teresa Kwamboka for prayers and daily prayers which kept me going during the entire period. To my brothers Samwel and Peter for the laughter shared

and always believing in me. I cannot be able to reward you effectively in a way that could be in tandem with the much support that you have given me. From me is to pray that God's grace may always abide with you, may you grow in kindness and continue impacting other lives positively. May the Good lord bless you abundantly.

ABSTRACT

Microplastics have become a notable concern in the context of plastic bottled drinking water. As plastic bottles degrade over time, they can release microscopic plastic particles into the water. This raises concerns about potential human exposure to microplastics and their associated health effects, therefore it has prompted researchers and regulatory agencies to investigate and set guidelines for the acceptable levels of microplastics in bottled drinking water to ensure consumer safety. This work delved into the characterization of microplastic particles in plastic bottled drinking water and analyzed the presence of heavy metals in plastic packaging through the utilization of two spectroscopic techniques: Raman Spectroscopy and laser-induced breakdown spectroscopy (LIBS) along with Principal component analysis (PCA). The Raman experimental parameters were: Excitation wavelength 785 nm and 532 nm; exposure time, 10s; spectra accumulation, 5; microscope objective, x100; 0.9 numerical aperture and 600 lines grating. The LIBS experimental parameters were: Excitation wavelength 1064 nm; laser power 250 mW; spectra acquisition mode, continuous; Pulse repeat frequency (PRF) 1Hz. A total of 14 different popular marque of plastic jarred drinking water from various manufacturing companies from local vendors in Narok and Nairobi counties were examined. Heavy metals were analyzed by cutting the packaging into small pieces measuring 2000 μm x 2000 μm and used LIBS for analysis. The water samples were filtered using Whatmann 1442-0.70 quantitative filter paper with a retention rate of 2.5 microns. We then utilized a Raman Optical Microscope BX51 to scan the filter paper and identify any plastic particles. Raman Spectroscopy and LIBS were employed to rapidly classify and identify the types of microplastics present, providing molecular and atomic information through scattered signals and plasma spectra. The analysis uncovered the presence of five distinct polymer types in the samples: Polypropylene (PP), polyvinyl chloride (PVC), polystyrene (PS) and Polyethylene terephthalate (PET). Among these polymers, polyethylene (PE) emerged as the most prevalent, appearing in 5 out of the 14 samples (35.71%). Polyethylene terephthalate (PET) followed as the second most common polymer, detected in 4 out of the 14 samples (28.57%). Polystyrene (PS) and polypropylene (PP) were each identified in 2 out of the 14 samples, while polyvinyl chloride (PVC) was found in only 1 sample. Furthermore, we calculated the C/H ratios for each polymer: PVC (0.89), PET (1.11), PP (1.17), PS (1.40) and PE (1.56). The trend observed in the C/H ratios is as follows: PE > PS > PP > PET > PVC. Furthermore, the study successfully detected and identified several heavy metals, including lead (Pb), antimony (Sb), mercury (Hg), uranium (U), manganese (Mn), zirconium (Zr), palladium (Pd), praseodymium (Pr), and thorium (Th), in the plastic packaging of the bottled water. Uranium was the most prevalent, appearing in 12 out of the 14 samples (86% prevalence), followed by mercury, which was present in 10 out of the 14 samples. Lead (Pb) was the third most prevalent, detected in 5 out of the 14 samples. The molecular spectra for polystyrene showed distinctive peaks at 999 cm^{-1} , 1028 cm^{-1} , 1601 cm^{-1} , 2899 cm^{-1} , and 3050 cm^{-1} and a C/H ratio of 1.18. The Raman spectra of the polystyrene standard sample exhibited no significant difference while being analyzed under 785 nm (250mW) and 785 nm (500 mW). The results are supported by a 3D scatter plot which clusters 250 mW and 500 mW together and segregates 785 nm and 532 nm respectively

Key Words: Microplastics, Laser Induced breakdown spectroscopy, Raman spectroscopy, Drinking water.

TABLE OF CONTENTS

DECLARATION AND APPROVAL	ii
DEDICATION	iii
ACKNOWLEDGEMENT	iv
ABSTRACT	vi
LIST OF FIGURES	xi
LIST OF TABLES	xiii
ABBREVIATIONS	xiv
CHAPTER 1.	1
INTRODUCTION	1
1.1 Background of the Study	1
1.2 Statement of The Problem	5
1.3 Objectives	7
1.3.1 General Objective.	7
1.3.2 Specific Objectives	7
1.4 Justification	7
CHAPTER 2	9
LITERATURE REVIEW	9
2.1 Introduction	9
2.2 Identification of Polymers Based on Atomic Signals	9

2.3 Microplastics in Drinking Water.	10
2.4 Methods Used in The Study of Microplastics.....	13
2.5 Suitability of LIBS for Elemental Analysis	15
2.6 Challenges with the Use of LIBS in Analysis of Liquids.....	16
CHAPTER 3	19
THEORETICAL BACKGROUND.....	19
3.1 Introduction.....	19
3.2 Prevalent polymers in water.....	19
3.3 Identification of Microplastics	21
3.3.1 Raman spectroscopy	21
3.3.2 Principle of Chemometric Techniques (PCA)	30
3.3.3 Laser Induced Breakdown spectroscopy (LIBS).....	29
3.4 Heavy Metals and Microplastics.....	31
CHAPTER 4	33
MATERIALS AND METHODS.....	33
4.1 Introduction.....	33
4.2 Sample Preparation	33
4.3 Measurement Techniques.	35
4.3.1 LIBS Measurements.....	35
4.3.2 Experimental Setup for LIBS Measurements	37

4.3.3 Raman Measurements	38
4.4 Spectral Data Preprocessing	40
4.5 Identification of the detected Microplastics.....	41
CHAPTER 5	43
DATA PRESENTATION, ANALYSIS, AND DISCUSSIONS	43
5.1 Introduction.....	43
5.2 Particle sizes of the detected Microplastics	43
5.3 Detection and Identification of Microplastics.....	46
5.3.1 Detection and identification of PE.....	46
5.3.2 Detection and Identification of PET	47
5.3.3 Detection and Identification of PP.....	48
5.3.4 Detection and Identification of PS.....	50
5.3.5 Detection and Identification of PVC.....	51
5.3.6 LIBS Atomic Spectra Lines	52
5.3.7 Average Number of C and H atoms and the C/H Ratios	54
5.4 Analysis of Heavy Metals.....	55
5.4.1 Detection of Pb and Sb	56
5.4.2 Detection of U and Hg	57
5.4.3 Detection of Mn and Na.....	58
5.4.4 Detection of Rare Earth Metals.....	59

5.3.5 Possible Human Health Effects of Heavy Metals.....	60
5.5 Raman and Laser Induced Breakdown Spectra for Polystyrene.....	63
5.5.1 Raman Spectra for Standard PS at 785 nm (250 mW and 500 mW).....	63
5.5.2 Raman Spectra for PS at 785 nm and 532 nm Laser Wavelengths	64
5.5.3 Raman Band Assignments for standard PS	65
5.5.4 Atomic Spectra for the Standard PS sample	67
5.5.5 Comparison Between the Standard and the Detected PS.....	68
5.5.6 Principal Component Analysis (PCA).....	70
CHAPTER 6	72
CONCLUSIONS AND RECOMMENDATIONS	72
6.1 Conclusions.....	72
6.2 Recommendations.....	73
REFERENCES	Error! Bookmark not defined.
APPENDICES	84

LIST OF FIGURES

Figure 3.1: Vibration Excitations from Raman Scattering	23
Figure 3.2: Polarized and Unpolarized Situations When an Electric Field is Present	25
Figure 3.3: A Classical Representation of Molecular Vibrations in A Diatomic Molecule	26
Figure 4.1: An image of LIBS2500Plus System (LIBS)	37
Figure 4.2: A Diagram for The Schematic Setup of LIBS for Bulk Water Analysis	38
Figure 4.3: A photograph Showing the STR Raman Spectrometer system.....	40
Figure 5.1: (a) Filter Paper Viewed Under 50x Magnification and (b) Filter Paper Viewed Under 100x Magnification.....	43
Figure 5.2: Filter Papers Showing Suspected Microplastic Particles Having Different Colors and Sizes (a) 24.4 μm (b) 34.4 μm (c) 53.44 μm (d) 63.3 μm	44
Figure 5.3: Different Images of Polystyrene Molecules Having Different Approximate Diameters (a) 20.31 μm (b) 19.66 μm (b) 18.36 μm and (d) 20.70 μm	45
Figure 5.4: (a) Spectra Obtained from Raman Analysis for Samples Containing Polyethylene (b) Spectra Acquired from LIBS Analysis for Samples Containing Polyethylene.....	47
Figure 5.5: The Spectra Collected from Raman Analysis for Samples Containing Polyethylene are Presented in (a), While the Spectra Obtained from LIBS Analysis for the Same Samples are Displayed in (b).	48
Figure 5.6: (a) Raman Spectra of Samples Containing Polypropylene (PP) (b) LIBS Spectra Obtained from Samples Containing Polypropylene (PP).	49

Figure 5.7: (a) Raman Spectra Obtained from Samples Containing Polystyrene (PS) (b) LIBS Spectra Collected from Samples Containing Polystyrene (PS).	50
Figure 5.8: (a) Raman Spectra Acquired from Samples Containing Polyvinyl Chloride (PVC) (b) LIBS Spectra Obtained from Samples Containing Polyvinyl Chloride (PVC).	51
Figure 5.9: Detection Wavelengths for Pb and Sb.....	57
Figure 5.10: Detection Wavelengths for U and Hg	58
Figure 5.11: Detection Wavelengths for Mn and Na.....	59
Figure 5.12: Detection Wavelengths for Rare Earth Metals.....	60
Figure 5.13: Raman spectra for Polystyrene Standard Sample Using 785 nm and Showing a Comparison Between 250 mw and 500 mW Laser Powers.	64
Figure 5.14:(a) Raman Spectra for Polystyrene Standard Sample Using 785 nm (250mW) and 532 nm (b) Raman Spectra for Polystyrene Standard Sample Using 785 nm (500mW) and 532 nm, They Highlight the Differences Between 785 nm and 532 nm Laser Wavelengths.....	65
Figure 5.15:Raman Spectra For PS at 785 nm and 532 nm Which Shows the Identified Raman Bands	67
Figure 5.16: Atomic Spectra for PS Standard Sample Showing the Detected Elements ..	68
Figure 5.17:(a) Raman Spectra for the Standard PS in Comparison with Raman Spectra from the Detected PS (b) LIBS Spectra for the Standard PS in Comparison with LIBS Spectra from the Detected PS	70
Figure 5.18: 3D Scatter Plot Showing PC Components for 785 nm and 532 nm.....	71

LIST OF TABLES

Table 3.1: Common Polymers Used in Day-To-Day Activities	19
Table 3.2: Chemical Formula, Structure and Raman Band Assignments for Common Polymers	28
Table 4.1: Spectrometer Modules for LIBS	36
Table 5.1: Atomic Spectra Lines That Were Identified in The LIBS Spectra	53
Table 5.2: Average Number of Atoms and C/H Ratios	55
Table 5.3: Possible Impacts of Heavy Metals on The Health of Humans.	62

ABBREVIATIONS

BPA	Bisphenol
EDS	Energy Dispersive Spectroscopy
FTIR	Fourier Transform Infrared Spectroscopy
IR	Infrared
LIBS	Laser Induced Breakdown Spectroscopy
MPs	Microplastics
NIR	Near Infrared Spectroscopy
PE	Polyethylene
PET	Polyethylene terephthalate
PS	Polystyrene.
SEM	Scanning Electron Spectroscopy
UV	Ultra violet

CHAPTER 1.

INTRODUCTION

1.1 Background of the Study

Over the recent years microplastics have gained global attention and presented themselves as a global challenge (Zainuddin & Syuhada, 2020). This is as a result of an increase in global production of plastics. Pollution from plastics is anticipated to rise in the near future as a result of lack of sustainable methods of handling them, further, increasing the burden on environmental conservation (Sommer et al., 2021). In the ocean alone the UN has reported an approximate of 51 trillion plastics particles. This number is 500 times greater than the number of stars in our milky way galaxy (Zainuddin & Syuhada, 2020). When these plastics are exposed to harsh environmental conditions, they break down to form microplastics.

Microplastics are particles that are insoluble in water and have diameters ranging between $1\mu\text{m}$ and $5,000\mu\text{m}$ (Tirkey & Upadhyay, 2021). These particles are broadly classified into two categories. The categories are based on size and the source of origin. Depending on the point of origin these particles can be put into two broad categories: primary and secondary. The primary particles are manufactured by industries intentionally at a micro metric range mainly for the purposes of cosmetics an example of these particles are the plastic pellets. On the other hand, secondary microplastics are not intentionally manufactured by industries but rather occur due to breakdown of plastic waste matter (Tirkey & Upadhyay, 2021). Plastic debris in our environment degrades as a result of

continuous exposure to thermal oxidation, bio film growth, exposure to UV rays, wave action and through mechanical shear (Andrady, 2017). Depending on the size of the particles microplastics can be categorized into two: large and small (Zainuddin & Syuhada, 2020). Large microplastics contain diameters lying in the range of 1-5000 μm , while small microplastics particles are ones whose diameters range from 1 μm to 1000 μm . Additionally, there are nano plastics, which have diameters below 1 μm (Tirkey & Upadhyay, 2021)

The continued weathering of microplastics leads to alteration in their chemical and physical properties (Rouillon et al., 2016). These properties include density, color, size, crystallinity and the morphology of the particle surface (Rouillon et al., 2016). Change of these properties further leads to harmful effects in our environment (Lambert & Wagner, 2016). For example, after weathering the microplastics can generally be yellow, tan colored or white (Tirkey & Upadhyay, 2021). These colors confuse the zooplanktons which tend to look at them as prey. The zooplanktons are later consumed by fish, which ends up being consumed as food by humans (Tirkey & Upadhyay, 2021). Research shows that the plastic packaging used to store drinking water also releases microplastics into the drinking water (Schymanski et al., 2018). Various studies have indicated that the microplastics have the ability to accumulate other toxic substances in their vicinity such as the hard metals. Compared to more recent microplastics, older ones have a tendency to amass a greater concentration of toxins (Wright et al., 2021). Microplastics can be able to leach from chemical functional additives added during the manufacture of plastics and can cause endocrine disruption as well as carcinogenesis, when humans ingest microplastics, these

particles can accumulate in various body tissues and organs, impacting the immune system and leading to various health complications (Rochman et al., 2014).

Drinking water being a vital resource for the survival of human beings needs to be free of contamination. The UN sustainable goal number six (SDG6) requires member states to work towards provision of clean water by the year 2030 (Costanza et al., 2016). The global consumption of plastic bottled drinking water has witnessed a significant rise in recent years, surpassing an annual per capita intake of 329.33 billion liters worldwide (Qian, 2018). This is also attributed by the safety concerns from other sources of water. While bottled drinking water boasts as a best choice for both personal and public consumption it poses various dangers to the consumers. First there are minimal regulations on bottled drinking water as compared to municipal water (Saylor et al., 2011). Secondly, plastic is the packaging material of choice by most manufacturers and most of the time it does not undergo recycling. The containers then end up to being junk in various dumpsites and as litter in our oceans, lakes and rivers. Overtime it disintegrates to smaller plastic fragments as a result of the methods mentioned in the antecedent paragraph.

Microplastics have widely been reported to be carriers for heavy metals and they interact in various ways, however these interactions are poorly comprehended (Liu et al., 2021). Heavy metals are naturally occurring; however, they can also arise from anthropogenic sources. They are widespread in the environment due to their nature of non-biodegradability. Microplastics and heavy metals pose a major threat to the environment as persistent pollutants. Microplastics, as a result of their small size and large surface area, act as magnets for toxic heavy metals and other pollutants. They have the capability to accumulate and concentrate these pollutants to elevated levels. Numerous studies have

reported heavy metal presence on microplastics, highlighting the concern of their coexistence and potential ecological impact (Prunier et al., 2019; Turner et al., 2019; Vedolin et al., 2018) Heavy metals being trace elements can be effectively studied using Laser Induced Breakdown Spectroscopy (LIBS).

The LIBS technique has achieved significant advancements in various fields such as food analysis, forensics, underwater sample analysis, waste management, and even in the realm of space exploration. This technique offers the capability to extract valuable information regarding both the elemental composition and molecular structure of the analyzed sample (Cheng et al., 2017). By utilizing laser ablation, a plasma is generated on the surface of the sample, which subsequently cools down and emits radiation specific to the elements present. These emitted radiations are then detected by a spectrometer. The LIBS technique boasts several advantages, including the ability to analyze samples regardless of their physical state, precise detection of surface contaminants, rapid analysis without the need for extensive sample preparation, and insensitivity to the surface morphology of the sample. Few studies have been done regarding the suitability of the technique in microplastic studies and the LIBS spectra is able to provide data that corresponds to vibrations and rotations of diatomic species in the generated plasma. However, the first study reporting the suitability of the technique in microplastic studies was reported by (Sommer et al., 2021).

In this study, LIBS and Raman spectroscopy were used along with Principal Component Analysis Chemometric method to detect and identify microplastics in plastic packaged drinking water. LIBS technique has been recognized for its rapid analysis and portability, making it suitable for in situ studies. On the other hand, the Raman technique depends on

scattered signal from the plastic, providing well-defined peaks for C-H and O-H, enhancing its analytical capabilities. It provides better identification compared to other methods such as NIR. PCA was used to visualize the complex dataset in a 2 and 3D scatter plot for identification of trends in the data. Little information is available especially on identification of plastics using elemental methods. These techniques have in recent studies delivered good results especially in the aspect of determination of additives and polymer types.

Due to the diversity of microplastics and the challenges of current techniques, there is a need for a spectroscopic method that can effectively cover their broad spectrum. LIBS has the ability to provide a clear distinction between microplastics and other natural materials based on the base polymer type. Raman is able to provide clear spectra on transparent microplastics. Hence a combination of these two techniques with a chemometric method can provide a comprehensive structural, molecular and elemental feature of microplastics. The combination could also complement any shortcomings from a single spectroscopic method.

1.2 Statement of The Problem

The consumption of bottled drinking water has become increasingly popular worldwide due to its convenience and concerns about the safety of other water sources. However, the comprehensive detection and analysis of microplastics in plastic bottled water have not been thoroughly explored according to existing studies. Further, analysis of heavy metals in the plastic packaging has not been comprehensively studied. There also lacks a standardized method for the detection and identification of these persistent pollutants. As the initial step towards removal of microplastics and heavy metals, accurate detection,

identification and classification is crucial. This study has addressed these gaps through the use of two spectroscopic methods and a chemometric technique to fully detect and identify microplastics in plastic bottled drinking water as well as analyze heavy metals in the plastic packaging. Through the study of the atomic spectra as a result of laser ablation from laser induced breakdown spectroscopy and molecular spectra from Raman spectroscopy as a result of scattering, microplastics and heavy metals have been characterized.

1.3 Objectives

1.3.1 General Objective.

To characterize microplastics in plastic bottled drinking water using Laser Induced Breakdown Spectroscopy (LIBS) and Raman Spectroscopy along with principal component analysis.

1.3.2 Specific Objectives

- i. To characterize microplastics in plastic bottled drinking water using Laser Induced Breakdown Spectroscopy and Raman Spectroscopy.
- ii. To analyze the presence of heavy metals in bottled plastic packaging using Laser Induced Breakdown Spectroscopy (LIBS).
- iii. To determine the Molecular and Atomic spectra for Polystyrene Microplastics using Raman Spectroscopy, Laser Induced breakdown spectroscopy and PCA.

1.4 Justification

Water is an essential component for existence of human beings. Its safety ensures reduced pandemic to humans as well as animals. Therefore, provision of safe and clean drinking water is basic human right and of the Millenium development goals (MDGs). Due to increased population, there is an increase in consumption of bottled drinking water in many countries across the globe. The most widely utilized type of packaging of such bottled water is plastic. These bottles are made from polymers and monomers which pose a great health risk especially from the additives which are susceptible to leaching (Lithner et al., 2011). Further, the plastic particles in consumable water, are a threat to the health of humans and their presence in the gut can lead to accumulation of other inorganic particles

and as a result cause severe health effect (Rochman et al., 2014). The studies on bottled drinking water are limited both in Africa and globally. This study, has investigated and provided a scientific understanding on the presence of microplastic particles in consumable water which was obtained from samples of bottled water. The obtained results are beneficial in development of policy and regulations by regulatory bodies towards ensuring water safety. This study has also contributed to the existing data on the suitability of the LIBS and Raman spectroscopy techniques in identification and chemical characterization of microplastics in drinking water especially for small particles sizes.

CHAPTER 2

LITERATURE REVIEW

2.1 Introduction

This chapter endeavors to present a comprehensive review of the pertinent literature that underpins this work at hand. This literature review establishes the current state of knowledge, identifies the gaps, and offers a critical analysis of existing research and theories.

2.2 Identification of Polymers Based on Atomic Signals

Different polymers can be distinguished on the basis of their C/H ratios obtained from the LIBS emission, (Gondal & Siddiqui, 2007) were able to distinguish between high density polyethylene (HDPE), Low density polyethylene (LDPE), PET, PP, PS and PVC studying the C atoms at 247.86 emission line and H atoms at 388.47 emission line. He used the two signals to fingerprint the five plastics and reported 1.68, 1.51, 1.01, 1.16, 1.42 and 0.91 as the C/H ratios for HDPE, LDPE, PET, PP, PS and PVC respectively. The study further identified Mn, Na, Sr and Mg using emission lines at 280.2, 588.9 nm, 500.9nm and 518.3 nm. Kim and Choi (Kim & Choi, 2019) were also able to differentiate between common household plastics by using the H α line at 656.3 nm and the C emission line at 247.9 nm. With these the study reported 1.03, 0.96, 1.42 and 1.19 for PP, ABS, PP, PET and PS respectively. The differences in the C/H ratios were used in the identification of the four common polymers. The study further identified He through the utilization of the emission line at 587.5 nm. In their study (Sattmann et al., 1998) were able to differentiate four common plastics using the C/H intensity ratios. The study analyzed the emission line for hydrogen at 486.13 nm and 247.86 nm for Carbon respectively. The study reported the C/H

Ratios 0.5, 0.5, 1.25 and 0.66 as the C/H ratios for PE, PP, PET and PVC respectively. This study was also able to identify PVC using the Cl emission line at 725.66 nm.

The obtained spectral lines are related to the concentrations of the samples that are emitting. The general appearance of the spectra obtained by LIBS for common plastics is similar, however the intensity ratios of the spectral lines for the elements are slightly different, this provides the basis for distinguishing between different types of microplastics using their C/H ratios.

2.3 Microplastics in Drinking Water.

The ingestion of microplastics is an issue of global concern. These particles have been found to pose various threats to the overall human health. Various studies have tried to determine the possible sources of microplastic ingestion, one of the possible sources has been found to be bottled drinking water (Schymanski et al., 2018; Winkler et al., 2019). The study of microplastics with their possible effects on human health is a field of interest. Microplastics have been found in air, beer, soil, in human stool and recently in human placenta (Gasperi et al., 2018; Kosuth et al., 2018; Shwabl et al., 2019; Antonio et al., 2021). These particles can either be inhaled or ingested. Oral consumption of microplastics is the most notable way of increasing their concentrations in human body and since they have the ability to accumulate toxic metals such as cadmium, lead and mercury which may exert toxicity by inducing immune response in the host body (Rochman et al., 2014). In the plastic manufacture process, some chemical supplements are added mainly to improve some properties like rigidity, flexibility, and resistance to UV rays. These additives such as Bisphenol A, Phthalates and alkylphenols are not bound to the plastic polymer chemically, hence are prone to leaching (Teuten et al., 2009). A possibility of intrinsic

chemical migration to the surface of microplastics as the degradation process continues cannot be ignored. Some of these additives such as Bisphenol A and Phthalates attack the hormone receptors thus affecting signal pathways. Bisphenol A (BPA) is known to affect estrogenic levels and on the other hand phthalates affects the testosterone levels. These additives can also lead to carcinogenesis (Teuten et al., 2009). Toxic levels of microplastics increases with reduction in their diameters, Polyethylene, Polystyrene and PET have been found to have cytotoxic effects in the human gastrointestinal tract. MPs can also move using the living cells into the circulatory and lymphatic systems leading to increased concentrations in organs such as spleen, liver and kidney (Kankanige & Babel, 2020).

The impacts of microplastics on the health of humans is an emerging area of interest. Different studies on bottled drinking water conducted using various methods have indicated presence of the microplastics in drinking water (Kniggendorf et al., 2019) detected presence of microplastics in streaming tap water. The research evaluated several tubing materials consisting of three polymers that are widely contained in microplastic researches over the world. They identified a direct source of microplastics as microbeads used in body care products and pellets from the fabrication of large plastics. In this study microplastics with sizes near to 0.1mm were detected with success and analyzed using Raman spectroscopy with 532nm laser activation energy. The tap water was flowing with 1L/h through a 3x3 mm² flow cell. The microplastics detected contained polyamide, polyethylene, polystyrene, polypropylene, and polymethyl-methacrylate (Kniggendorf et al., 2019).

In a separate investigation, (Mintening et al., 2019) conducted a study with the primary aim of identifying microplastics in underground drinking water sources. The study

meticulously analyzed 2,500 liters of water collected from groundwater sources. Notably, microplastics within the size range of 50 to 150 micrometers (Mintenig et al., 2019) were successfully detected during the research. The identified microplastics encompassed polymers such as Polyamide (PA), PE, Polyester (PES) and PVC. The examination employed 0.2 micrometer filters coated with aluminum and used the FTIR-Micro Spectroscopy technique.

In another study, (Mason et al., 2018) conducted an extensive study focusing on the potential presence of synthetic polymer contamination in bottled water. The work encompassed the analysis of 11 different samples of packaged water collected globally, specifically investigating contamination from microplastics. Two methods, namely FTIR Spectroscopy and Nile Red tagging, were employed in a combined approach to achieve this. The study revealed an average contamination level of 325 particles per liter (Mason et al., 2018). Various polymers were identified and presented in form of percentages. Among them, PP was reported to be the prevalent polymer, accounting for 54% of the total, followed by Polyamide (PA) at 16%, Polystyrene at 11%, and Polyethylene at 10%, although not as prominently (Mason et al., 2018). Additionally, the study discovered that a significant proportion, 95%, of the detected particles were smaller than 100 micrometers. In conclusion, the study emphasized that packaging could potentially serve as a source of contamination.

In their study, (Schymanski et al., 2018) investigated various types of packaged drinking water, including reusable and single-use glass bottles, as well as plastic bottles. The primary aim of the research was to identify small microplastics and assess the potential release of plastic particles in micro range from the packaging into the mineral water. The

study revealed that small microplastics ranged from 50 to 150 micrometers, while very small microplastics fell within the same size range (Schymanski et al., 2018). In analyzing these plastic particles in the samples of bottled drinking water, Raman Spectroscopy was employed. The Raman spectrometer utilized gold-coated polycarbonate filters and operated at 532nm wavelength. Each sample consisted of 100ml. The research identified Polyester (PES), Polyamide (PA) and Polyethylene terephthalate (PET) as the detected microplastics. Conclusively, the study highlighted that packaging could serve as a potential source of contamination (Schymanski et al., 2018).

In the investigation of pigmented particles and small microplastics in bottled water (Oßmann et al., 2018) did notable study. The study sampled 32 different brands of mineral water in glass and plastic bottles. Raman spectroscopy at 532 nm was used with polycarbonate membrane coated in aluminum that had a filter pore size of 0.4 micrometers. In the study 250ml sampling volume of each sample was used. It was observed that Polyethylene terephthalate (PET) was rampant in plastic bottles whereas Polypropylene (PP) and Polyethylene (PE) were dominant in in glass bottles. In addition to microplastics detected a polymer named Styrene-butadiene was also found in glass bottles. In conclusion it was reported that Microplastics contamination might have originated from cleaning, refilling as well as packaging processes (Oßmann et al., 2018).

2.4 Methods Used in The Study of Microplastics

Several techniques have been employed for both characterization and sampling of microplastics. Characterization techniques include Near-Infrared Spectroscopy (NIR), Raman spectroscopy, Scanning Electron Microscopy with Energy Dispersive X-ray

Spectroscopy (SEM-EDS), Fourier Transform Infrared Spectroscopy (FTIR), Photoluminescence (PL) spectroscopy and Nuclear Magnetic Resonance (NMR) (Tirkey & Upadhyay, 2021). Microplastic sampling techniques comprise visual sorting, density separation, sieving, filtration, and acid digestion (Sommer et al., 2021; Tirkey & Upadhyay, 2021). FTIR is the most commonly used method for identifying the chemical composition of microplastics. It operates on the principle that when a sample containing microplastics are shone with infrared (IR) radiation, they absorb the radiation, which is then measured during transmission or reflection. The absorption depends on the molecular structure of each individual microplastic (Saylor et al., 2011). This method detects the carbonyl group (a polar functional group) by causing alteration in the dipole moments of the sample's bonds upon IR absorption (Tirkey & Upadhyay, 2021). FTIR is preferred due to its nondestructive nature, reliability, and directness (Ojeda et al., 2009). However, it is limited to dry samples and samples larger than 10 micrometers in size (Sommer et al., 2021), and the presence of irregular particles can cause scattering and reduce efficiency in the reflection mode (Ornik et al., 2020).

Another method that has gained popularity is the Raman spectroscopy. This technique utilizes vibrational spectra which works on the principle of inelastic scattering of light (Araujo et al., 2018). The method has the ability to obtain the chemical structure of the sample and thus providing a chance for identification of the constituent particles in the sample. The technique is mainly applied in the identification of microplastics because of its ability to distinguish between small particles, its high sensitivity to non-polar functional groups and low interference from (Tirkey & Upadhyay, 2021). As a result of its high sensitivity the technique can be able to identify particles with diameters less than 1 μm by

providing their structural and chemical characteristics. This makes it advantageous as compared to FTIR spectroscopic (Tirkey & Uipadhyay, 2021)). However, this technique is time consuming in that it needs rapid sample preparation and data processing thus posing difficulties for in situ measurements (Sommer et al., 2021).

Another method is the Near Infrared Spectroscopy (NIR). This method works on the principle that when a sample containing microplastics is irradiated with NIR radiation, they absorb the electromagnetic radiation and the molecules produce vibrations. The materials are then identified based on their different vibrational characteristics. This technique poses a greater potential in identification of microplastics in that it has a greater penetration power as compared to FTIR and no sample preparation is required (Tirkey & Uipadhyay, 2021). However, the current technique has limitations as it can only identify microplastics larger than 1mm in diameter. A more recent method employed for microplastics identification is the photoluminescence technique. This technique relies on the principle that materials, when optically stimulated, emit light upon returning to their ground state. Photoluminescence spectroscopy has been successfully utilized for identifying microplastics in marine environments, employing 405 nm as the excitation wavelength. However, there is some overlap in the observed bands, making it difficult to clearly differentiate between various types of plastics (Ornik et al., 2020).

2.5 Suitability of LIBS for Elemental Analysis

In their study (Chen et al., 2020) utilized LIBS to characterize heavy metals present in microplastics. This study demonstrated that LIBS method can be used for robust analysis of heavy metals in single microplastics and to determine their concentrations. The study also indicated the ability of LIBS to simultaneously analyze many elements in a short

period without the sample pretreatment. However, in this study the LIBS technique was integrated with bright-field microscopy. The heavy metals were detected with only one laser shot. The research indicated that the technique is promising especially in the study of pollutants that use the microplastics as vectors for migration from one geographical location to another.

In another study (Sommer et al., 2021) investigated the ability of LIBS in carrying out microplastic identification. In the study seven plastic types were used as reference which included; polyethylene terephthalate, polystyrene, polycarbonate, polythene, polyamide, polyvinyl chloride and propylene. These plastics were further divided into aliphatic (PP, PE, PVC) and aromatic plastics (PS, PET, PC). This study used a Q-switched Nd: YAG laser with a wavelength of 1064 nm, a frequency of 10 Hz. The laser was able to produce total energy of 200 mJ with a pulse width of 4 ns. The study observed clearly defined spectra for plastics and non-plastic materials. The polymer types were identified based on a decision tree which was on the basis of the emission ratios between involved molecules and chemical constituents.

2.6 Challenges with the Use of LIBS in Analysis of Liquids

The LIBS has had uses in various areas. It has been mainly used for analysis of solids, gases and liquids. The technique has the ability to carry out elemental analysis and provide both quantitative and qualitative data. For all the three types of matter the gases and solids have had a bigger share in terms of preference by scientists. The liquids on the other hand still rank last (Sommer et al., 2021). The analysis of liquids poses various technical challenges which have to be overcome for successful analysis. During the analysis of liquids bubbles are produced when the laser interacts with the liquid sample (Charfi &

Harith, 2002). Also, shockwaves are produced which results in spluttering of the liquid (Yueh et al., 2002). A study conducted by (Zhang et al., 2018), found out that the bubbles result in change of the laser magnitude and the spectra that is collected consequently. On the other hand, the spluttering of the laser contaminated solution can lead to contamination of the optical equipment. This therefore, leads to time wastage in frequent and thorough cleaning of the optical components.

However, several tactics have been employed in order to avoid splashing of the laser contaminated solution as well as production of bubbles when the laser beam interacts with the liquid solution. Thakur and Singh (Thakur & Singh, 2020) proposed the utilization of a Liquid Jet method in the examination of liquid samples using LIBS technique whereas (Ruas et al., 2017) in their experiment on the application of LIBS to Zirconium in Aqueous Solution proposed analysis of a liquid sample using a bulk method approach. Another notable proposal in alleviating these technical difficulties in analyzing liquid samples, (Lazic et al., 2017) in their experiment used the approach of freezing the liquid solution. They also proposed reduction of frequency to 1Hz in order to improve reproducibility of spectral measurements and avoid splashing. The liquid sample's stability can be improved if parameters such as flow rate can be looked upon (Cheng et al., 2017). Although the proposed methods improve reproducibility, sensitivity and efficiency of data acquisition is reduced as a result of rapid sample preparation involved (Zhang et al., 2018).

Given the adverse impacts associated with microplastics, it is crucial to develop methods for their detection and identification in bottled drinking water, facilitating their removal. However, there are limited works focusing on the analysis of microplastics in bottled drinking water using combined LIBS and Raman spectroscopy. Furthermore, these studies

have not explored the simultaneous application of both spectroscopic methods on the same sample for microplastic analysis. By utilizing both spectroscopic techniques, it is possible to complement each other's strengths, leading to more accurate results. For this work, we utilized LIBS elemental signals from various samples to calculate C/H ratios, which assisted in identifying the base polymers present in microplastics. Raman spectra signals have also been collected for the same samples for complete identification of the microplastics on the basis of their molecular vibrations and elemental compositions. LIBS has also been applied in analysis of heavy metals in plastic packaging that are used to carry the water and results presented thereof.

CHAPTER 3

THEORETICAL BACKGROUND

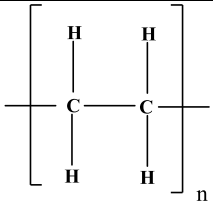
3.1 Introduction

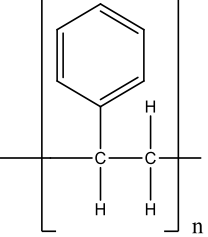
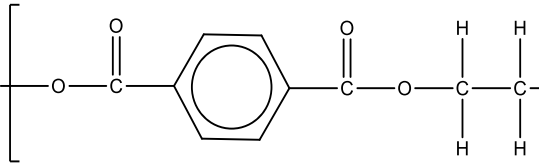
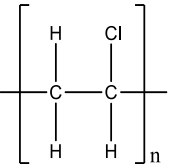
This chapter aimed at elucidating the theoretical underpinnings of the present work, outlining the most common polymers, principles of spectroscopic methods, the relationship and interactions between heavy metals and microplastics and chemometric method (PCA) to inform the analysis and lend depth to the research findings.

3.2 Prevalent polymers in water

Table 3.1 illustrates the prevalent polymers frequently detected in water samples, namely PE, PET, PP, PS and PVC (Nava et al., 2021; Schwarz et al., 2019). Table 3.1 provides insight into their chemical structures, applications, and potential impacts on human health.

Table 3.1: Common Polymers

Type of Polymer	Chemical Structure	Use	Possible Health Effects
Polyethylene (PE)	 $\left[\begin{array}{cc} \text{H} & \text{H} \\ & \\ -\text{C} & -\text{C}- \\ & \\ \text{H} & \text{H} \end{array} \right]_n$	Packaging bottles.	Ingestion can cause damage to the liver (Hu et al., 2022)

<p>Polystyrene (PS)</p>		<p>Manufacture of single use coffee cups.</p>	<p>Inflammation of the liver (Lei et al., 2018) Can cause death of human cells (apoptosis) (Shen et al., 2021)</p>
<p>Polyethylene Terephthalate (PET)</p>		<p>Manufacture of plastic bottles.</p>	<p>Leads to microbiota dysbiosis (Shen et al., 2021)</p>
<p>Polyvinyl Chloride (PVC)</p>		<p>Manufacture of water pipes.</p>	<p>Can change the genes (Gondal & Siddiqui, 2007) Causes cancer (Blackburn</p>

			& Green., 2022.)
Polypropylene (PP)	$\left[\begin{array}{c} \text{CH}_3 \quad \text{H} \\ \quad \\ -\text{C} - \text{C}- \\ \quad \\ \text{H} \quad \text{H} \end{array} \right]_n$	Manufacture of food packaging	It has the ability to stimulate cytokines, which can lead to inflammation. (Hwang et al., 2021)

3.3 Identification of Microplastics

Microplastics can be identified using either atomic or molecular spectra. In the current study Raman spectroscopy and laser induced breakdown spectroscopy have been used.

3.3.1 Raman spectroscopy

This is a powerful non-destructive method that can be used in analyzing molecular properties of matter which operates on the principle of light scattering. This technique makes use of anti-stokes and stokes scattering in order to determine the molecular structures of matter (Raja & Barron, 2019). When an electromagnetic radiation in the range of near infrared or visible light interacts with matter three types of scattering come into play. One thing that is common about all of them is that an incident photon having energy E as shown in equation (3.1) makes the molecule to rise from a lower vibrational state to

another virtual state which is located between first electronic state and the ground state (Lohumi et al., 2017).

$$E = h\nu \quad (3.1)$$

Scattering depends on the way a molecule relaxes after it has been excited. The molecular vibration mechanisms can be fully discussed using principles of quantum and classical physics.

3.3.1.1 Quantum Explanation of Raman scattering

There are three types of scattering in Raman spectroscopy which include; Stokes, Rayleigh and anti-stokes scattering. For Rayleigh scattering the molecule becomes excited to an infinite virtual state but later relaxes to its original state. In this case the photon remains with its original energy and hence the photon is said to have been scattered elastically (Kosuth et al., 2018). For stokes scattering the photon is scattered inelastically and it leaves with an energy E given by equation (3.2).

$$E = h\nu - \Delta E \quad (3.2)$$

In this scattering the molecule starts from an original state, it gets excited to a much higher state but later falls back to a state that is lower than the state which it originally started from. In the anti-stokes scattering the photon becomes excited super elastically in that it possesses an energy E given by equation (3.3).

$$E = h\nu + \Delta E \quad (3.3)$$

The molecule begins from an excited state, it becomes excited to a higher state but later falls to a vibrational state that is much lower than its original state (Gardiner, 1989). The three types of scattering and the changes in electronic states are shown in Figure 3.1.

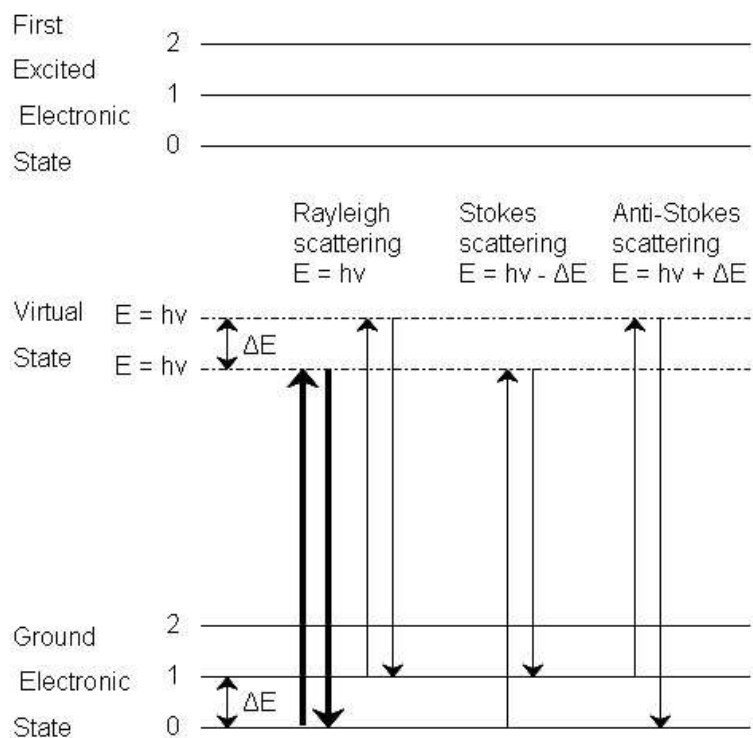


Figure 3.1: Vibration Excitations in Raman Scattering (Oßmann et al., 2018)

As shown in Figure 3.1, Rayleigh scattering is the predominant form of scattering, where there is no alteration in the molecule's vibrational state. In contrast, anti-Stokes scattering necessitates the molecule to be initially in a vibrationally higher state before interacting with the photon. Consequently, anti-Stokes scattering is less commonly employed due to this requirement. On the other hand, Stokes scattering is the most common scattering used in Raman measurements because anti Stokes scattering has low intensity and for Rayleigh scattering, a lot of filtering is required so as to exclude photons having incident energy or even higher (Winkler et al., 2019). Raman spectroscopy takes into consideration changes

in the energy between the scattered photons and the incident photons which are associated to both stokes and anti-stokes transitions. Raman measurements are done in terms of changes in the wavenumber from the incident photons and thus light of any wavelength can be used. The primary internal vibrational coordinates encompass various motions. These include stretching, which alters the length of a bond; bending, which modifies the angle between two bonds; rocking, which causes a shift in the angle within a group of atoms; and wagging, which induces a change in the angle for a specific group of atoms. Additional coordinates include twisting, which changes the angle between two groups of atoms, and out-of-plane, which involves altering the angle of a single atom with respect to the others. (Raja & Barron, 2019).

Raman spectroscopy is also dependent on how a bond is polarized. Polarizability measures the ease to which a bond can be deformed by an electric field. Polarizability is also dependent on how ease a bond can be displaced which in return induces a temporary dipole. Concentration of loose electrons is proportional to polarizability and large polarizability translates to an intense Raman signal. Raman spectroscopy is thus important in fingerprinting of organic molecules since the vibrations are highly specific to a given molecule as a whole. (Raja & Barron, 2019).

3.3.1.2 Classical theory of Raman Scattering

On the basis of classical physics Raman scattering relies on the polarizability of the molecules. According to (McCreery, 2005) a laser beam can be viewed as an electromagnetic wave which is oscillating with an electrical vector E . Molecular deformation which are the main basis of this technique are determined by the polarizability α which is given by equation (3.4).

$$P = \alpha E \quad (3.4)$$

Polarizability depicts the tendency of a molecule or an atom to undergo a change in its electron distribution as a response to an external electric field. This is shown in figure 3.2.

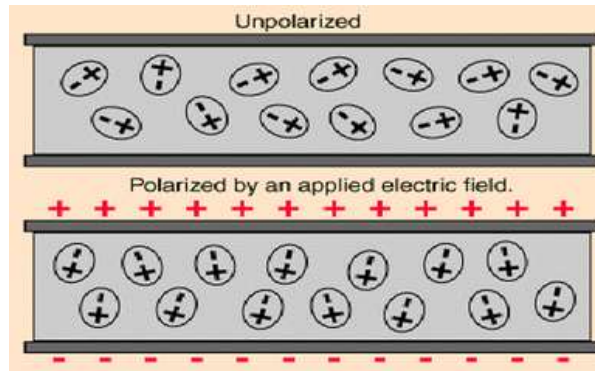


Figure 3.1: Polarized and Unpolarized Situations When an Electric Field is Present (Lazic et al., 2017)

When a laser beam is shone on a plastic sample, an electric dipole moment is induced which leads to deformation of the molecules. As a result of this deformation the molecules vibrate with frequencies that are characteristic to each individual molecule (McCreery, 2005).

These vibrations in materials can also be explained using the Hooke's theory and in this case the atoms are taken as point masses and the bonds that connect them represent an elastic cord with negligible weight as shown in figure 3.3 (Oreborn, 2018).

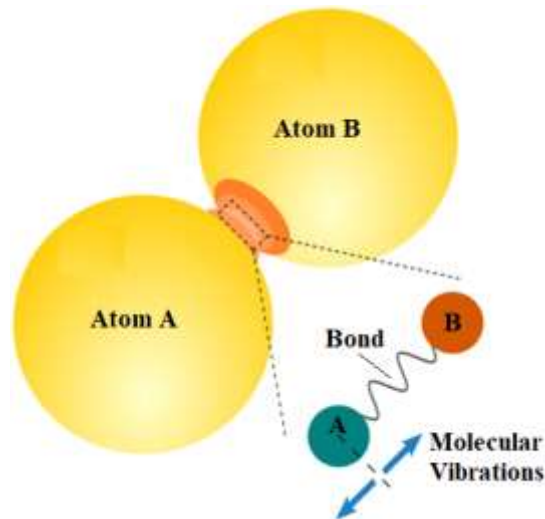


Figure 3.2: A Classical Representation of Molecular Vibrations in A Diatomic Molecule (McCreery, 2005).

From the Hooke's law the vibrational frequencies of the bond can be approximated using the equation 3.5 below (Siebert & Hildebrandt, 2008).

$$f = \sqrt{\frac{F}{M}} \times \frac{1}{2\pi C} \quad (3.5)$$

where; f is the vibrational frequency given in wavenumber

C stands for the speed of light

F represents the force exerted by the bond and its constant

M is the reduced mass of the atoms.

A net shift in the 1st derivative of α (polarizability) of the molecular vibrations cause Raman active vibrations. The vibrations caused are with respect to the normal coordinate q as shown in the equation 3.6 below (Leng, 2009)..

$$\left(\frac{d\alpha}{dq}\right) q = 0 \neq 0 \quad (3.6)$$

Where $q = \frac{\mu}{E}$

μ represents the molecule's induced dipole moment of the molecule that causes the scattering of the incident light.

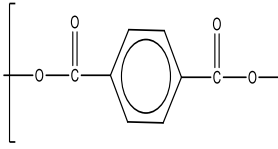
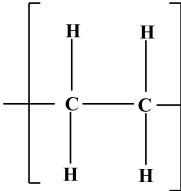
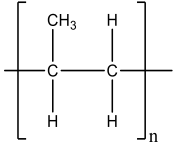
E stands for the electric field (external) that causes the polarizability of the molecule.

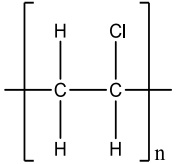
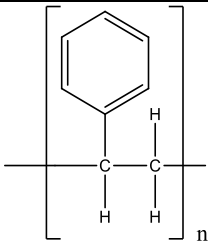
Moreover, the polarizability of the molecules varies with the length of the bonds and are confined to discrete vibrational energies as shown in figure 3.1.

3.3.1.3 Vibrational Spectra of Common Polymers

The chemical structure of microplastics is often altered by the presence of additives or continuous degradation. This may cause an alteration to the Raman spectra which will result in misidentification especially by using the spectra libraries. It is therefore of utmost importance to know the main peaks of the most common plastics. The bands are essential in comprehending the chemical fingerprints of the polymers. Table 3.2 highlights the Raman band assignments that is essential in fingerprinting microplastics.

Table 3.2: Chemical Formula, Structure and Raman Band Assignments for Common Polymers

Polymer	Chemical Formula	Chemical Structure	Raman Vibrational frequency (cm ⁻¹)	References
Polyethylene terephthalate (PET)	(C ₁₀ H ₈ O ₄) _n		278, 626, 701, 800, 857, 950, 1000, 1096, 1119, 1192, 1295, 1310, 1418, 1462, 1615, 1730, 2912, 2968, 3085	(Shameem et al., 2017; Nava et al., 2021; Rebollar et al., 2014)
Polyethylene (PE)	(C ₂ H ₄) _n		1062, 1130, 1170, 1295, 1417, 1440, 1460, 2850, 2883	(Nava et al., 2021; Furukawa et al., 2006; Ghosal et al., 2018; Di & Wang, 2018)
Polypropylene	C ₃ H ₆) _n		252, 321, 398, 458, 530, 809, 841, 900, 941, 973, 998, 1040, 1102, 1152, 1167,	(Shameem et al., 2017; Nava et al., 2021; Andreassen,

			1219, 1257, 1296, 1306, 1330, 1360, 1371, 1435, 1458, 2840, 2871, 2883, 2905, 2920, 2952	1999; Guo et al., 2019; Khafagy, 2006)
Polyvinyl chloride (PVC)	$(C_2ClH_3)_n$	 <p>The diagram shows the repeating unit of Polyvinyl Chloride (PVC) enclosed in large square brackets with a subscript 'n'. Inside the brackets, two carbon atoms are connected by a single bond. Each carbon atom is also bonded to two other atoms: one hydrogen atom (H) and one chlorine atom (Cl). The carbon atoms are also bonded to the continuation of the polymer chain, indicated by horizontal lines extending from the brackets.</p>	310, 345, 363, 420, 496, 544, 571, 599, 615, 638, 682, 694, 752, 838, 930, 964, 972, 1066, 1101, 1119, 1172, 1187, 1216, 1257, 1316, 1335, 1357, 1379, 1430, 1437 , 1498, 2914, 2935, 2969, 2994	(Baibarac et al., 2021; Ludwig et al., 2018)
Polystyrene (PS)	$(C_8H_8)_n$	 <p>The diagram shows the repeating unit of Polystyrene (PS) enclosed in large square brackets with a subscript 'n'. Inside the brackets, two carbon atoms are connected by a single bond. Each carbon atom is also bonded to two other atoms: one hydrogen atom (H) and one phenyl ring (represented by a hexagon with a circle inside). The carbon atoms are also bonded to the continuation of the polymer chain, indicated by horizontal lines extending from the brackets.</p>	621, 795, 1001, 1031, 1155, 1450, 1583, 1602, 2854, 2904, 3054	(Shameem et al., 2017; Nava et al., 2021; Mazil u et al., 2010)

3.3.2 Principle of Chemometric Techniques (PCA)

Raman spectra can be obtained with relative ease; however, its interpretation is quite tricky and for this reason it is essential to incorporate chemometric methods. The datasets obtained are complex and large making it difficult to extract important information and trends. Chemometric methods make use of mathematical and statistical tools to get important information from complex datasets to achieve the desired qualitative information (Potcoava et al., 2014). In this study we mainly focused on PCA (Principal component analysis) for carrying out Multivariate data analysis.

PCA is a mathematical method that identifies the directions that have maximum variance in a complex dataset and reduces the dimensions of the data for easier visualization. The principal components are perpendicular to each other and they capture the largest variation inside the provided data. The first principal component gives the most variance, the second PC gives second most variance and the third PC gives the third most variance and so on. The primary purpose of PCA is to determine which directions the data shows greater variance. The eigenvectors of the covariance matrix which are associated with the largest eigen values dictate these directions and the magnitude of the eigen values indicates the amount of variance that is present in the data along the various eigenvector directions (Mishra et al., 2017). PCA operates by making clusters of data which have similar spectral profiles. In order to achieve this the original data is projected on principal components (Ondieki, 2020). For example, if Z is a $\mathbf{m} * \mathbf{n}$ matrix PCA reduces it to;

$$Z = XY^T \quad (3.7)$$

Where,

X represents the first principal component PC1 ($\mathbf{m} * \mathbf{r}_{\max}$)

\mathbf{Y}^T represents the transpose of the matrix Y in an ($\mathbf{n} * \mathbf{r}_{\max}$) matrix and depicts Principal Component 2, PC2;

\mathbf{r}_{\max} displays the components number that is equal to the X rank.

Apart from reducing the dimensionality of the dataset PCA also shows the outliers and the covariance between different samples. The PCA loadings show important qualitative information that enables effective identification of the molecular bands present in the Raman data (Ondieki, 2020).

3.3.3 Laser Induced Breakdown spectroscopy (LIBS)

When a laser beam of a small diameter is directed on the liquid sample in a small. The laser's huge irradiance breaks down the sample (Novotný et al., 2014). Particles of the liquid sample gain energy and hence are excited as a result of energy absorption; the chemical bonds are broken to an atomic or ionic level. Free electrons then gain further energy through inverse Bremsstrahlung. Ionization then increases rapidly; the result of this rapid ionization is the development of a plasma with an electron bulk of about 10^{17} to 10^{20} cm^{-3} and temperature $^{\circ}\text{C}$ of about 10^3 to 10^4 (Novotný et al., 2014). When the laser energy becomes greater than the threshold energy required, the plasma with high density and temperature is created in that portion. In the plasma the molecules, atoms and ions spread in various levels, move from high to low energy levels discharging a strong Spectra. The emission magnitude from the disintegrated species then provides the elemental composition of the liquid sample contaminated with microplastics. Electromagnetic waves analogous to a distinctive wavelength of individual element are discharged from the high-strung atoms. The spectra emitted is then utilized to establish elemental components of the measured sample

It is crucial to recognize that the LIBS signal is directly linked to the concentration of the identified elements in the analyzed water samples. When a laser beam interacts with the sample, it generates a plasma that contains excited atoms or ions. The LIBS technique focuses on analyzing this plasma to obtain emission spectra unique to each element present in the sample. In an optically thin and homogeneous spectrum, the intensity of a spectral line I is produced by an excited atom or ion (Gondal & Siddiqui, 2007).

$$I = h\nu_{ji}A_{ji}N_j \quad \text{where } i = 0,1,2,3,\dots \text{ And } j = 1,2,3, \dots \quad (3.8)$$

Where,

I , represents the spectral line intensity

h represents the Planck's constant

N_j = is the population in the upper-level j

A_{ji} = is the Einstein coefficient that corresponds to spontaneous emission

ν_{ji} = stands for the transition frequency from j to i states.

The case of thermodynamically equilibrium energy levels is as shown in equation 3.9 (Gondal & Hussain, 2007).

$$N_j = N g_j Q^{-1} \exp\left(-\frac{E_j}{kT}\right) \quad (3.9)$$

Where g_j = stands for energy of the upper-level j

E_j = represents the statistical weight

k = stands for Boltzmann constant

Q = represents the specie's partition function

T = represents temperature of the electron in the plasma

According to (Gondal & Hussain, 2007), If we combine equation (i) and (ii) we get

$$I = h \nu_{ji} A_{ji} N g_j Q^{-1} \exp\left(-\frac{E_j}{kT}\right) \quad (3.10)$$

By utilizing Equation (iii), we can ascertain the atom's population density associated with any element present in the LIBS spectra. This determination is achieved through the

understanding of atomic constants, the excitation temperature, and the measurement of intensity.

3.3.3.1 The C/H Ratios

Carbon and Hydrogen play an essential role in the structures of the polymers. In the identification of polymers which are the building blocks for microplastics, different approaches can be employed which include: calculation of C/H ratios, the use of pattern recognition in the cases where standard samples are present or using statistical techniques (Kim & Choi, 2019; Unnikrishnan et al., 2013). The difference in C/H intensity ratios is brought about by the difference in C-H and C-C bonds. For the common plastics. PET is the only one that contains an oxygen functional group and hence can be identified easily. On the other hand, PVC also contains the Cl emission line which can also be used as a distinctive feature.

3.4 Heavy Metals and Microplastics

Plastics can be said to be a cocktail of contaminants because they are made up of various pollutants that have been sorbed from the surroundings. Some of these contaminants include 78% of priority pollutants such as Pb (Rochman et al., 2014). More than half of all the polymers that are produced contain chemicals which have been characterized by the UN as hazardous. The presence of other organic pollutants and heavy metals on plastic fragments has been well established. The presence of hard metals on plastics is attributed primarily to both the manufacturing process and environmental sorption. Plastic containers, in particular, have been observed to accumulate heavy metals from the sample waters they hold (Ashton et al., 2010; Rios et al., 2010; Fischer et al., 2010).

The mechanism of interaction between heavy metals and microplastics is commonly explained by the influence of electrostatic interactions, π - π interactions and van der Waals forces (Torres et al., 2021; Liu et al., 2021) Microplastics have been found to have a zero-charge pH point, this indicates that in a natural environment they are negatively charged on their surface. Heavy metals are positively charged and hence there is attraction between the positively charged heavy metals and the negatively charged microplastics which is electrostatic in nature. This electrostatic attraction promotes adsorption behavior. The polymers that contain oxygen groups have been shown to have an increased polarity of the Microplastics and thus making them more reactive (Holmes et al., 2012). This then will lead to an increase's capacity of adsorption of the heavy metals. This adsorption is also dependent on the on the pH value, a higher pH value means increased adsorption capacity to heavy metals and vice versa (Guo et al., 2020). For instance, when the pH value is below 3, the surface of microplastics, such as polyethylene (PE), acquires a positive charge, resulting in low electrostatic repulsion and zeta potential. This suggests that negatively charged heavy metal ions like CrO_4^{2-} will be drawn towards the microplastic surface. Conversely, as the pH of the microplastics increases, their surface becomes negatively charged, attracting positively charged heavy metals to it (Liu et al., 2021).

CHAPTER 4

MATERIALS AND METHODS

4.1 Introduction.

In this chapter an overview of the techniques utilized for sample preparation, characterization, and identification of microplastics and heavy metals is discussed. The sample preparation process involved acquiring the samples from various outlets in Nairobi and Narok counties in Kenya. The characterization of the collected samples involved the use of techniques Laser-induced breakdown spectroscopy (LIBS) and Raman spectroscopy, both available at the Laser Lab in the Department of Physics, Faculty of Sciences and Technology, University of Nairobi. LIBS was used for elemental analysis, while Raman spectroscopy provided insights into the molecular composition of the microplastics that were detected in the samples.

4.2 Sample Preparation

The collection of samples involved procuring one and half liters of plastic bottled water from various vendors in Narok and Nairobi Counties. Fourteen replicate samples were obtained, representing plastic bottled water from different manufacturing plants in Kenya. To prepare each sample for analysis, a Whatman 1442 – 070 quantitative, Ashless, grade 42 filter paper was used for filtration of 1 liter for each sample. This filter paper was composed of high-quality cotton linters with specific characteristics including a wet burst of 0.40 psi, a filtration speed of 1870 seconds /100 ml of water, a diameter of 70 mm, a thickness of 200 μm , a pore size of 2.5 μm , an ash content of less than 0.007 %, and a basis weight of 100 g/m^2 . The filtered papers were then placed individually in labeled petri dishes and left to air dry overnight under room temperature. This sample preparation procedure

was specifically conducted for Raman spectroscopy measurements. In contrast, no sample preparation was required for Laser induced breakdown spectroscopy (LIBS) measurements, which utilized a time-grating detection technique to eliminate any continuum emissions from the sample. For LIBS measurements, a volumetric approach was employed. Equal volumes were measured using a beaker that was cleaned with distilled water. Specifically, 100 milliliters of the bottled water were poured into a holder made of glass for analysis using a laser beam. Following analysis, the holder was rinsed with distilled water to minimize contamination before proceeding with the next sample. This process was iterated for all the fourteen samples each four times until all of them were analyzed.

For examination of heavy metals in the plastic packaging, three pieces measuring 2000 μm by 2000 μm were accurately cut randomly from the plastic bottles that contained the water samples which were analyzed. A sterilized vernier caliper was used to do the measurement, in mm then the units were converted to μm . The bottle cap, the bottom and the middle of the plastic bottle were chosen for extraction using a new surgical blade. These parts were a representation of the whole plastic bottle. For each plastic bottle a total area of 12000 μm^2 was randomly analyzed for the selected heavy metals. The extracts were then placed in different plastic petri dishes ready for analysis. Since Laser Induced breakdown spectroscopy technique was used in this case no further sample preparation was needed. The procedure was repeated for all the fourteen plastic bottles from which water had been filtered out.

The Polystyrene Standard sample analyzed was in suspension form. The sample was siphoned using a sterilized syringe and needle to minimize contamination. The medium

sized droplets were placed on top of glass slide wrapped with aluminum foil. The droplets were labelled PS1, PS2 and PS3. They were then allowed to dry for 10 minutes before being taken for analysis using Raman and LIBS spectroscopy.

4.3 Measurement Techniques.

The samples were studied for molecular vibration and elemental composition. The identification of microplastics was done using confocal Raman spectroscopy by looking at their base polymer types while the detection and elemental composition were done using Laser induced breakdown spectroscopy.

4.3.1 LIBS Measurements

The examination of heavy metals and detection of microplastics were conducted using Laser-Induced Breakdown Spectroscopy (LIBS). Specifically, the Ocean Optics LIBS2500Plus Laser-Induced Breakdown Spectrometer system was utilized for these measurements. The experimental parameters included: laser source; Q-Switched Big Sky Laser Quantel, pulse width; 8ns, laser energy; 250 mJ, Pulse Repeat Frequency (PRF) 1Hz and 1064 nm as the center wavelength. For each pulse a calculated 31.25 MW peak power was provided with the laser operating on a 1-second period. This system enabled the real-time qualitative analysis of trace elements. The system allowed analysis of the spectra between 200-980 nm providing a resolution ~ 0.1 nm (FWHM). The sensitivity of the equipment was in parts per billion. The system consisted of seven spectrometer channels and operated with a 32-bit Windows XP PC. The spectrometer modules are provided in the table 4.1;

Table 4.1: Spectrometer Modules for LIBS

Channel	Range in nm
UNIT A-HR+C0463	198.16-302.59
UNIT B-HR+C0464	295.71-391.72
UNIT C-HR+C0465	384.98-514.01
UNIT D-HR+C0466	503.54-620.74
UNIT E-HR+C0467	617.40-722.65
UNIT F-HR+C0468	715.71-804.65
UNIT G-HR+C0469	797.08-971.11

The LIBS2500Plus system operated using the OOILIBSplus version 4.5.0.7, developed by Ocean Optics. This application offered features such as spectral saving, data logging, and laser firing control. Additionally, the software was integrated with correlation software that facilitated real-time detection and identification of elements during system operation. The LIBS2500Plus system also included a library of spectra comprising 2,500 atomic intensity lines gotten from the National Institute of Standards and Technology (NIST). These intensity lines contributed in simplifying the calibration and identification processes for the LIBS2500Plus system. Figure 4.1 illustrates the LIBS2500Plus system.



Figure 3.1: An image of LIBS2500Plus System (LIBS) which was utilized in this study (Photo credits to the Laser Lab, UON, Kenya). The Part named A indicates a spectrometer module, B- Big Sky Laser Quantel Laser, C- Sample analysis chamber, D- Laser power system, E- CPU, F-LCD monitor

4.3.2 Experimental Setup for LIBS Measurements

The collimated beam from the pulse laser was focused into the sample (bottled drinking water contaminated with microplastics) using a lens and directed into the sample. The generated plasma was collected using a plano-convex lens and with the utilization of a fiber collimation package the collected plasma was analyzed with a LIBS2500plus spectrometer. The delay time was then controlled by a digital delay generator. It was also used to produce the trigger-pulse for the laser and the spectrometer. This proposed study utilized the bulk method of analysis whereby samples were analyzed in a bulky manner as shown in the figure 4.2 below.

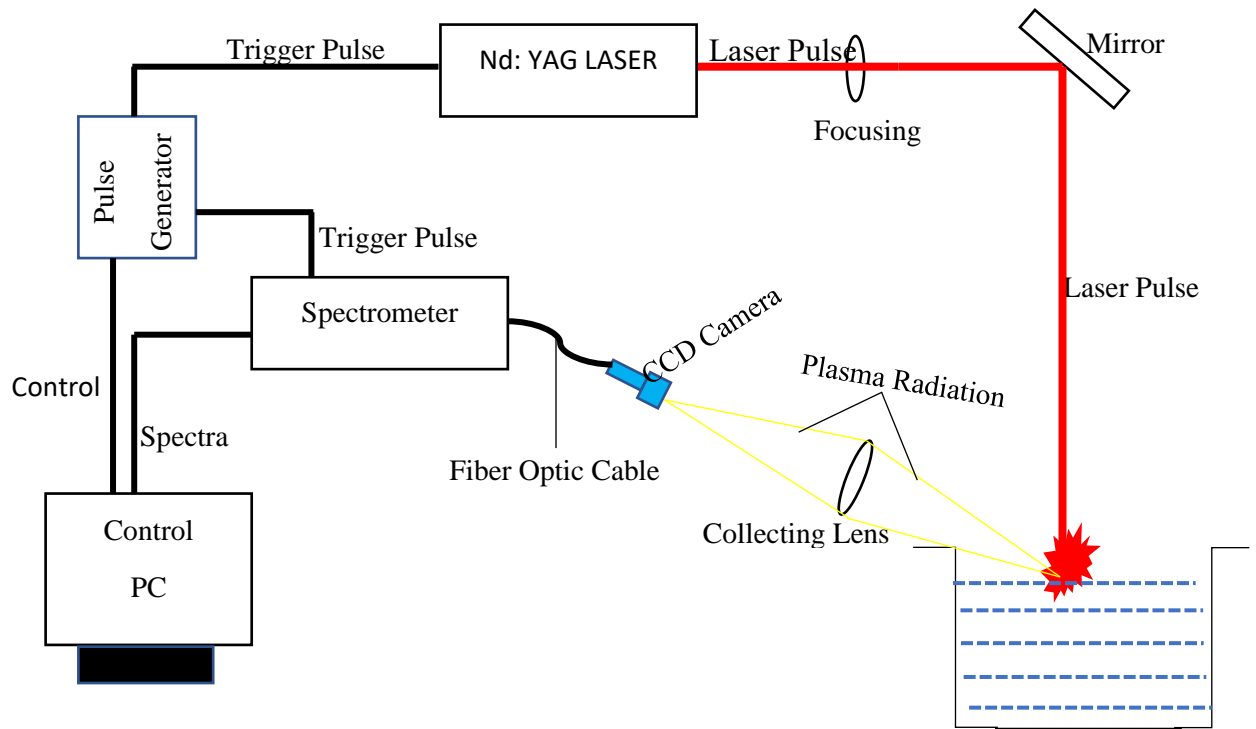


Figure 4.2: A Diagram for The Schematic Setup of LIBS for Bulk Water Analysis

4.3.3 Raman Measurements

Raman Spectroscopy was employed to analyze the vibrational modes of the microplastics in this study. The Sinuze Tarun Raman Spectrometer (STR Raman spectrometer) was utilized, which consisted of a Laser Quantum gem laser with 532 nm wavelength and a 785 nm He-Ne laser. The excitation source had frequency ranging between $50\text{-}4000\text{ cm}^{-1}$ and 2.0 cm^{-1} resolution. The laser had a center wavelength of 600.54 nm, and each spectrum was captured with 10 seconds and 10 as exposure time and accumulations respectively. The STR Raman system, manufactured by Seki Technotron Japan, comprised Raman optics equipped with two 532 nm filters, Neutral density (ND) filter, mirrors and a 50/50 beam splitter. The ND filter allowed for the maximum intensity (100%) of the laser to be

used. Additionally, the system included an Olympus BX51 confocal optical microscope, featuring an objective lens with 100x magnification and a numerical aperture of 0.90. The objective lens was selected to provide optimal resolving power, with a value of 0.00384. Spectra was processed using an SP2300 Acton Spectrometer having an 0.300 m imaging Triple grating monochromator made by Princeton Instruments. The spectrographs were plotted in terms of intensity and wavenumbers, utilizing the 600Blz grating among the available gratings (1800Blz, 1200Blz, and 600Blz). The weak Raman signal was detected using the Pixis 256 CCD detector, working at -75 °C. Raman software version 1.41.3 made ARix Corp was employed for spectrum acquisition. Prior to measurements, the calibration of the STR Raman system was done using a silicon wafer which was aligned with the commonly known 520.5 cm^{-1} spectrum. The sample was positioned on a stage and adjusted using the stage controller to ensure accurate measurements. The stage controller was connected to the confocal Raman Microscope system. The power delivered to the sample at a wavelength of 532 nm, utilizing the 100x objective lens, was measured to be 1.886 mW.

The laser Spot size at 532 nm wavelength was approximately 721 nm. The spectra acquisition mode was set to accumulate at 10 and the acquired spectra was displayed on a 21.6 Acer LCD monitor operating on windows 7. For each sample three particles were viewed randomly using the microscope. Their images were taken using the Raman Microscope camera and their diameters estimated at 100x magnification. For each particle 5 spectra were taken randomly across the particle and their spectra saved. This procedure was repeated for all the fourteen filter papers representing the fourteen samples. The

measurements were taken in a dark room between 8 am and 5 pm to minimize interference from the background.



Figure 4.3: A photograph Showing the STR Raman Spectrometer system (Photo credits of the UON, Kenya). The part named A depicts 532nm laser, B- Raman optics system, C- 21.6-inch Acer LCD display, D- STR Raman controller system (CPU), E- The stage control system, F- Stage, G-Optical table H-Confocal Raman Microscope unit. I- Acton Sp2300 spectrometer system, J- Pixis 256 CCD Detector, K-UPS system.

4.4 Spectral Data Preprocessing

Data analysis was done using Origin Pro 2021 (64-bit open-source software) made by OriginLab Corporation. For the Raman measurements, the analysis steps included averaging, baseline subtraction, smoothing, normalization of the curves and peak finding. Averaging was done for all Raman data representing each observed particle. For baseline

subtraction the baseline mode was set to user defined and points were chosen smoothly on the graph, the 2nd derivative (zeroes) anchor points finding method was used with an adjacency-Averaging smoothing. The points were connected by interpolation method and for this case line interpolation method was chosen for easy selection of the points. For smoothing of the spectral graphs, the Savitzky-Golay method with 5 points of window, no boundary condition and a polynomial of order 2 were used. The graphs were then normalized to [0,1] with a manual recalculate method. For finding peaks the baseline was first defined and the peaks were filtered based on their height. The threshold height was automatically set to 20%.

Principal Component Analysis (PCA) was done on the preprocessed Raman data to uncover spectral patterns inside the dataset. This technique allowed for the visualization of associations between different observations with minimal information loss. Specifically, PCA was conducted on spectra data obtained from the 785 nm and 532 nm wavelengths. The study utilized a standard polystyrene sample, and each dataset consisted of ten spectra. In the case of LIBS measurements, data analysis involved several steps. This included baseline subtraction, smoothing, normalization of curves, and peak labeling. The obtained LIBS spectra were utilized to calculate the C/H ratios for each polymer type. The average C/H ratio was determined using equation 4.1 (Gondal & Hussain, 2007).

$$\text{Average C/H Ratio} = \frac{\text{Total number of C-atoms at 247.8nm}}{\text{Total number of H-atoms at 388.4nm}} \quad (4.1)$$

4.5 Identification of the detected Microplastics.

For Microplastics identification the processed spectra were compared to various spectra from the target polymers (PP, PVC, PET, PS and PE) from various studies. This was done

for the processed Raman data since the STR Raman used for this experiment had no inbuilt library. Various characteristic bands for all the polymers were obtained. Most of the plastic molecules contain additives, some have been subjected to degradation while others have been coated with other residues that are organic. Hence there is a probability of obtaining and altered Raman spectra of most polymers. This then makes it difficult to use the automatic procedure of comparing the obtained spectra with ones available from spectral libraries. The knowledge of the main peaks that are characteristic to many polymers thus came in handy. This did not only increase accuracy but also reduced the chances of misidentification of the polymers. For this study the main peaks of the various polymers of interest (PE, PVC, PET, PS and PET) were thus obtained from various works of literature and compared with the obtained spectra for identification of the polymers as shown in table 2 presented in ensuing chapters.

CHAPTER 5

DATA PRESENTATION, ANALYSIS, AND DISCUSSIONS

5.1 Introduction

In this chapter a comprehensive examination of the experimental results is provided. The data obtained from Raman spectra, plasma spectra for the identified microplastics, and plasma spectra for the identification of heavy metals in plastic bottled water packaging are thoroughly examined.

5.2 Particle sizes of the detected Microplastics

The particles of interest for this work were ones lying in the micro to millimeter range that is between 2.5 μm to 5mm, this is the accepted definition of microplastics. The control filter paper that had not been contaminated with microplastics is shown in figure 5.1

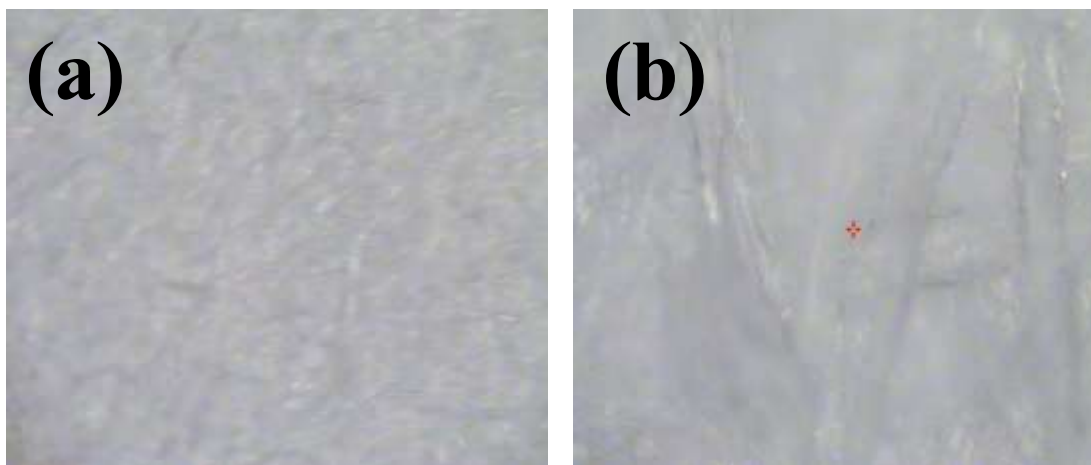


Figure 5.1 :(a) Filter Paper Viewed Under 50x Magnification and (b) Filter Paper Viewed Under 100x Magnification.

The particle sizes as measured using the STR Raman software measuring tool indicated that the particles ranged between 20 μm and 63 μm . These particles were very small and could not be seen with the naked eye. The particles had various colors which could have contributed to the detected fluorescence. The particles are shown in figure 5.2

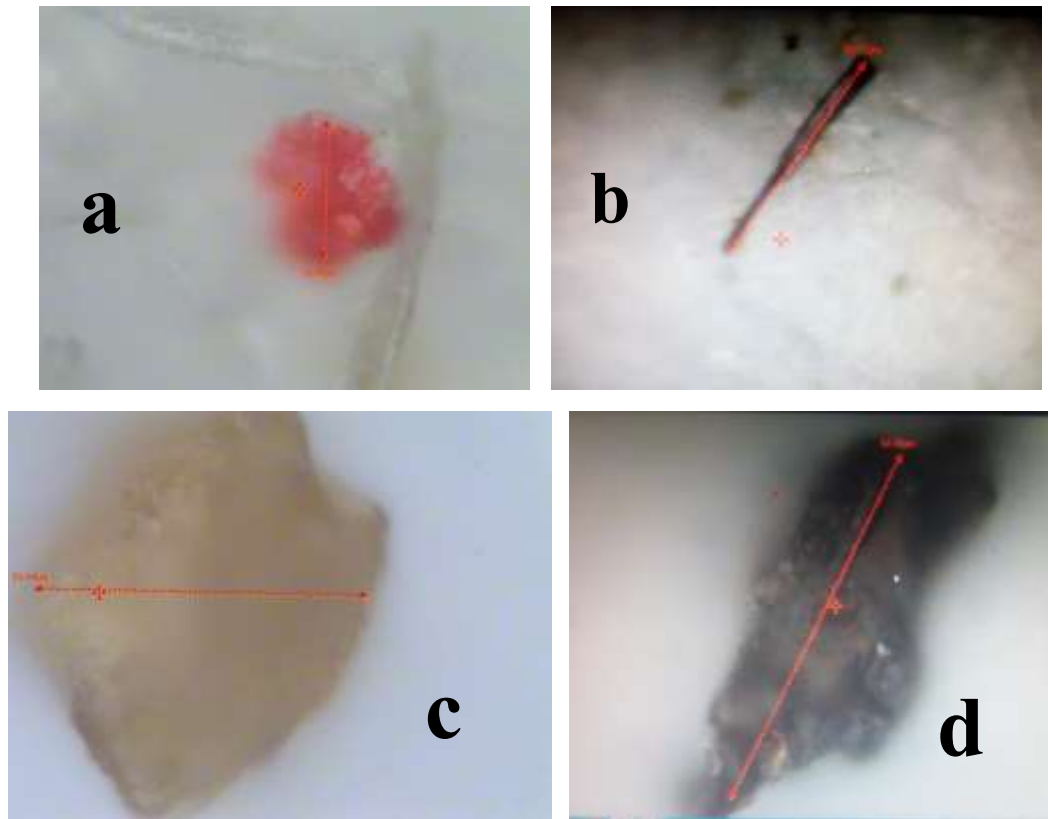


Figure 5.2: Filter Papers Showing Suspected Microplastic Particles Having Different Colors and Sizes (a)24.4 μm (b) 34.4 μm (c)53.44 μm (d) 63.3 μm .

The crystals for the standard polystyrene sample are also shown in figure 5.3

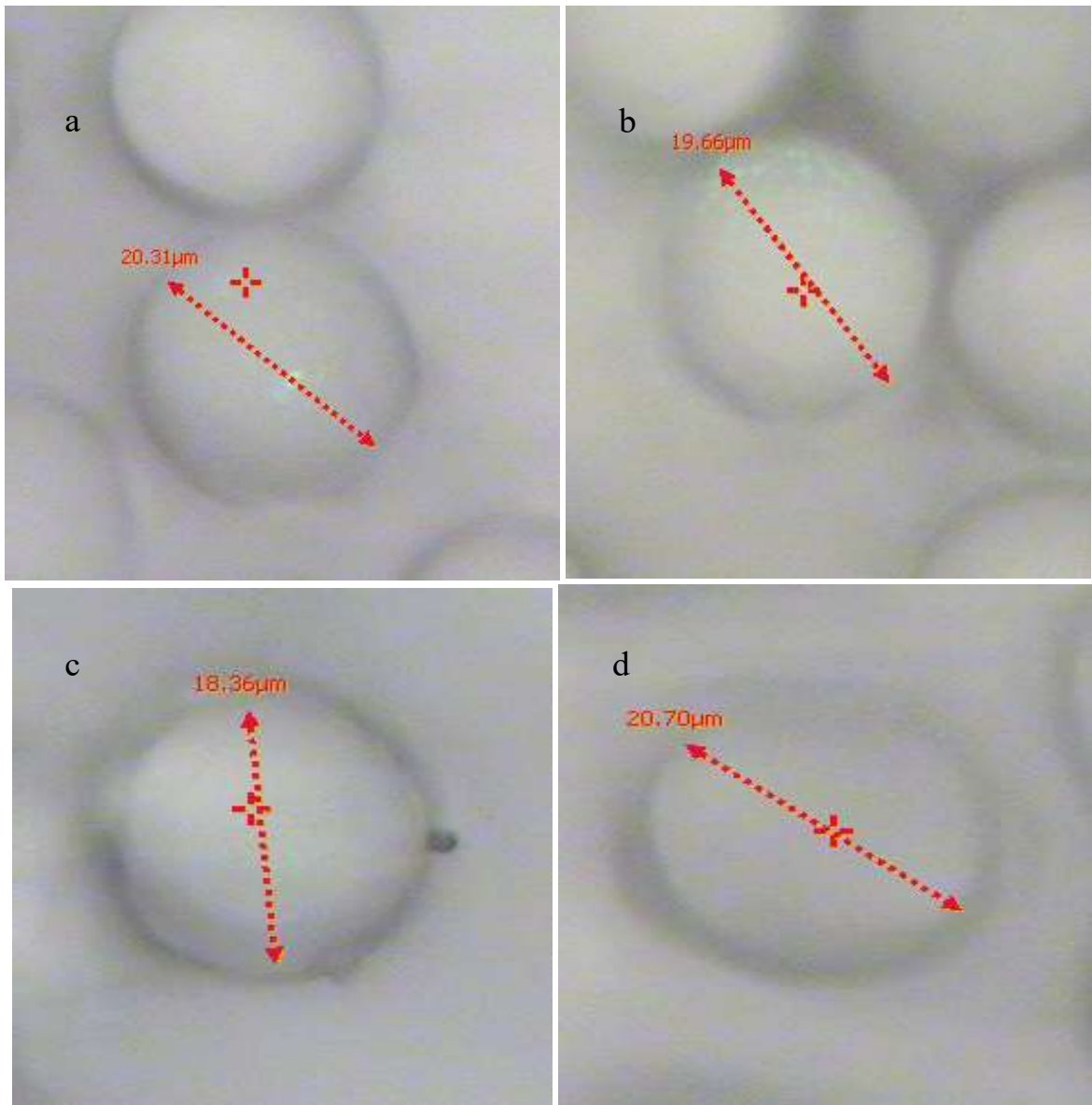


Figure 5.3: Different Images of Polystyrene Molecules Having Different Approximate Diameters(a) 20.31 μm (b) 19.66 μm (b) 18.36 μm and (d) 20.70 μm

5.3 Detection and Identification of Microplastics

The polymers of interest included both aromatic (Polystyrene) and aliphatic (PP, PE, PVC) types (Grégoire et al., 2011). The Raman measurements provided vibrational spectra that confirmed the existence of particular polymers inside the water samples analyzed. Furthermore, the LIBS measurements captured atomic spectra, which were utilized to assess the C/H ratios of the polymers.

5.3.1 Detection and identification of PE

Distinct Raman bands were identified at specific wavenumbers in five of the 14 samples. These bands encompassed peaks at 1129 cm^{-1} and 1063 cm^{-1} , which correspond to the stretching of the single C-C bonds. Additionally, a peak at 1169 cm^{-1} is associated to the rocking vibration of CH_2 , while the presence of 1291 cm^{-1} indicated CH_2 twisting vibration. Moreover, the signal at 1442 cm^{-1} represented CH_2 bending vibration, whereas the peaks at 2884 cm^{-1} and 2850 cm^{-1} signified asymmetric and symmetric stretching of CH_2 , consequently, as illustrated in Figure 5.4 (a). These discernible bands closely align with the characteristic vibrational modes of Polyethylene (Nava et al., 2021; Furukawa et al., 2006; Ghosal et al., 2018; Di & Wang, 2018). Figure 5.4 (b) illustrates the LIBS spectra for these 5 samples. The average CH ratio among these samples was determined to be 1.56. The higher C/H value is attributed to the elevated density resulting from the level of crystallinity in PE, which aligns closely with the findings of (Edition, 2011), further confirming the presence of polyethylene.

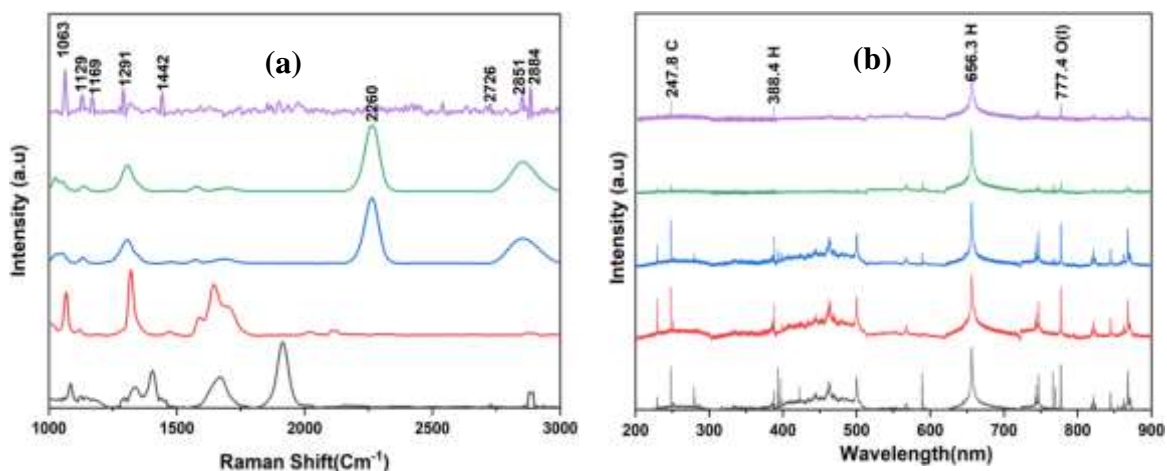


Figure 5.4: (a) spectra obtained from Raman analysis for samples containing polyethylene (b) spectra acquired from LIBS analysis for samples containing polyethylene.

5.3.2 Detection and Identification of PET

Among the total of fourteen water samples, distinct Raman bands were observed in four of them. Specifically, the signal leading to 858 cm^{-1} peak is linked to the vibrations of C-(O)-O and C-C bonds which are stretching. An additional band at 1096 cm^{-1} is attributed to the antisymmetric stretching vibrations of (C-O-C) bonds. Moreover, the band located at 1118 cm^{-1} is connected to C-C single bond inside ethylene glycol and C(O) bond. Furthermore, a peak at 1185 cm^{-1} signifies the vibrations due to C-C bonds which are stretching, while the band at 1295 cm^{-1} is indicative of the vibrations of C(O)-O stretching bond. Additionally, the band observed at 1420 cm^{-1} originates from the bending vibrations involving O-CH, CH_2 , and C-CH bonds. Meanwhile, the peak positioned at 1615 cm^{-1} correlates to vibrations associated with 8a ring mode in the Wilson notation. Lastly, the band at 1739 cm^{-1} is linked to the vibrations of C=O stretching bonds. These distinctive Raman bands have been visually represented in Figure 5.5 (a). Their presence is characteristic of Polyethylene Terephthalate (Shameem et al., 2017; Nava et al., 2021;

Rebollar et al., 2014). Figure 5.5 (b) displays the LIBS atomic spectra of the four samples. The mean C/H ratio found for these samples was 1.11, which aligns closely with the findings of (Gondal & Siddiqui, 2017; Sattmann et al., 1998). This supports further the existence of PET in the analyzed samples.

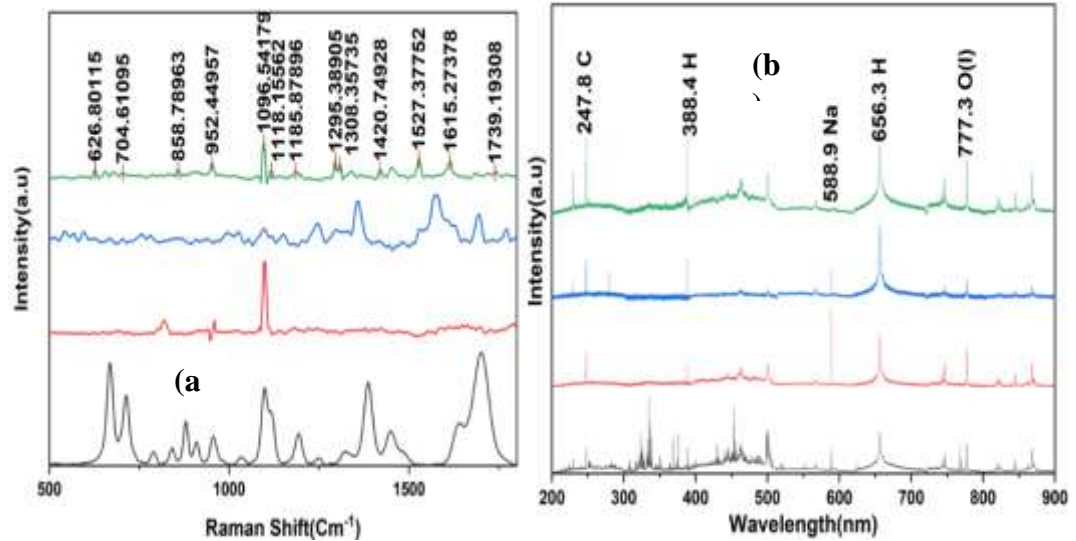


Figure 5.5: The Spectra Collected from Raman Analysis for Samples Containing Polyethylene are Presented in (a), While the Spectra Obtained from LIBS Analysis for the Same Samples are Displayed in (b).

5.3.3 Detection and Identification of PP

Raman bands were detected in two out of the fourteen samples, exhibiting distinct vibrational patterns. At around 398 cm^{-1} , the observed band is attributed to the bending vibrations of CH bonds and the wagging of CH_2 bond. Another band at 809 cm^{-1} signifies CH_2 vibrations (rocking), C- CH_3 and C-C bond vibrations (stretching). Additionally, at 841 cm^{-1} , the band arises from the vibrations (rocking) of CH_3 and CH_2 , as well as the vibrations due to C- CH_3 and C-C stretching bonds. Band at 984 cm^{-1} indicates rocking vibrations of CH_3 and stretching vibrations arising from C-C bonds. The vibrations of C- CH_3 and C-C

stretching bonds, along with the vibrations of the CH bending bond, contribute to the band at 1040 cm^{-1} . Moreover, the peak at 1164 cm^{-1} is associated to the bending of CH bonds and the rocking vibrations of CH_3 . Noteworthy Raman bands also occur at 1468 cm^{-1} and 1320 cm^{-1} resulting from CH and CH_2 bending vibrations, the twisting of CH_2 and asymmetric bending of CH_3 . These reported Raman peaks are visually represented in Figure 5.6 (a). These particular vibrational patterns are characteristic of PP (Shameem et al., 2017; Nava et al., 2021; Andreassen, 1999; Guo et al., 2019; Andradý, 2017; Khafagy, 2006). Figure 5.6 (b) displays the elemental spectra captured through LIBS measurements for the two samples. The average C/H ratio obtained for these two samples is 1.17. Polypropylene contains repeating units of methyl groups and substituted methylene groups, which align with these findings. The obtained ratio closely resembles the results obtained by (Kim & Choi, 2019; Gondal & Siddiqui, 2017), further confirming the presence of Polypropylene.

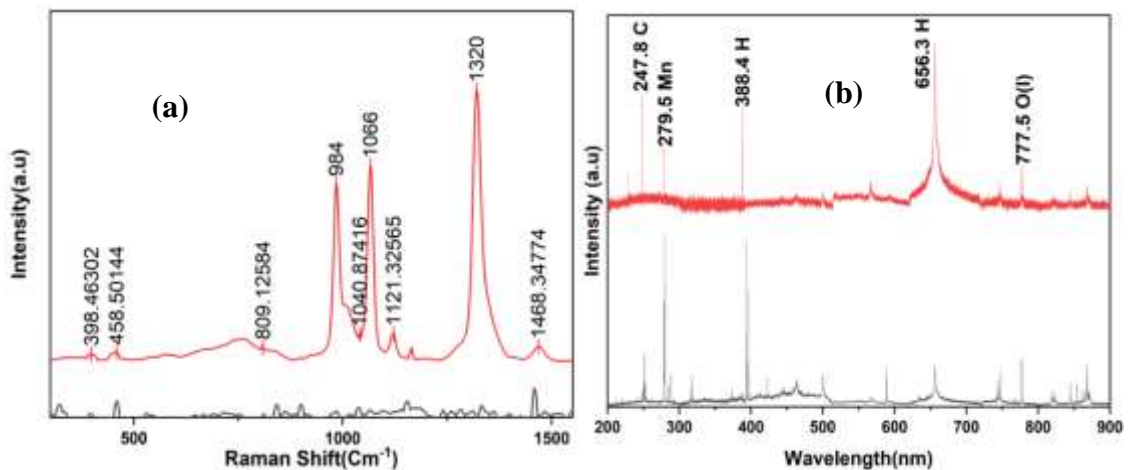


Figure 5.6: (a) Raman Spectra of Samples Containing Polypropylene (PP) (b) LIBS Spectra Obtained from Samples Containing Polypropylene (PP).

5.3.4 Detection and Identification of PS

Distinctive Raman bands were observed in two more samples out of the complete set of fourteen. At around 622 cm^{-1} , the observed band is linked to deformation of the benzene ring. A notable band at around 1001 cm^{-1} originates from the ring's breathing mode of the aromatic carbon. The peak at 1031 cm^{-1} is attributed with CH deformation (in-plane). Moreover, the peak at 1155 cm^{-1} is attributed to stretching vibrations of C-C bonds, while the band at 1451 cm^{-1} is ascribed to scissoring vibrations of CH₂. Additionally, the band situated at 1602 cm^{-1} signifies the ring's skeletal structure vibrations (stretching). These discernible peaks are visually shown in Figure 5.7(a). They are indicative of the characteristics of (PS) (Shameem et al., 2017; Nava et al., 2021; Mazilu et al., 2010). Figure 5.7(b) presents the LIBS spectra obtained from the two water samples. The mean C/H fraction was determined to be 1.40, which agrees with the findings of (Gondal & Siddiqui, 2017). This further supports the presence of polystyrene in the samples.

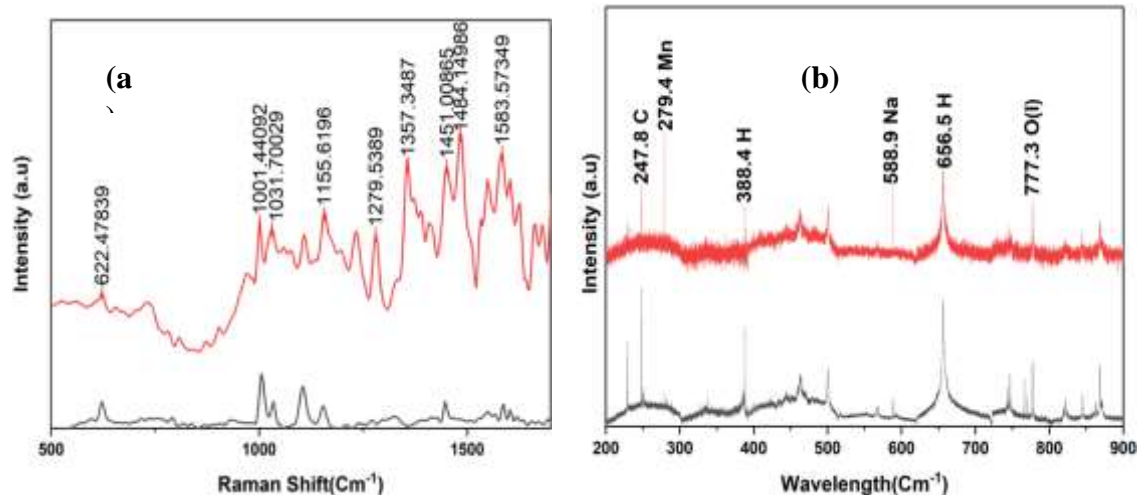


Figure 5.7: (a) Raman Spectra Obtained from Samples Containing Polystyrene (PS) (b) LIBS Spectra Collected from Samples Containing Polystyrene (PS).

5.3.5 Detection and Identification of PVC

Characteristic peaks were also detected in one of the fourteen samples as shown in figure 5.8. The band at 361 cm^{-1} is attributed to C-Cl bond inside the PVC polymer undergoing trans configuration. Additionally, the peak at 612 cm^{-1} correlates to of C-Cl stretching bond vibration. The band at 695 cm^{-1} signifies the vibrations of C-Cl bonds. Moreover, the band at 1395 cm^{-1} arises from the symmetrical stretching of C-H bonds in the CH_2 group, while the band at 1430 cm^{-1} is arises from C-C bonds stretching. These observed peaks are displayed in Figure 5.8(a). The peaks show existence of PVC molecule in the sample (Baibarac et al., 2021; Ludwig et al., 2018). PVC has various additives, hence accounting for the presence of unknown bands (Nava et al., 2021). Figure 5.8(b) shows the acquired LIBS spectra, where the mean C/H ratio was determined to be 0.89. This value closely aligns with the findings of (Gondal & Siddiqui, 2017; Sattmann et al., 1998), further indicating the existence of PVC.

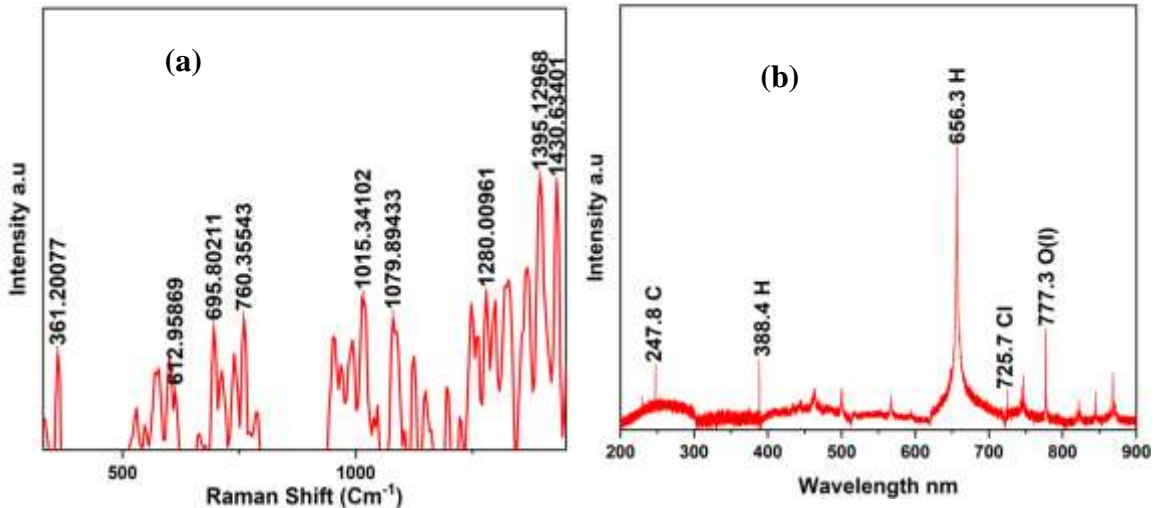


Figure 5.8: (a) Raman Spectra Acquired from Samples Containing Polyvinyl Chloride (PVC) (b) LIBS Spectra Obtained from Samples Containing Polyvinyl Chloride (PVC).

5.3.6 LIBS Atomic Spectra Lines

Table 5.1 offers a concise overview of the atomic emission lines that have been recognized in LIBS measurements, each associated with distinct characteristic wavelengths. The selection of these particular spectral lines is rooted in their heightened intensity, which serves to notably minimize interference stemming from other emission lines. Furthermore, these chosen lines do not include transitions from the lowest state, thus ensuring the trivial impact of self-absorption. Within the realm of LIBS measurements, one notable atomic line at 247.8 nm correlates to a transition from the $2s^22p^2$ state to the $2s^22p^3s$ state. The atomic line positioned at 388.4 nm stands as a distinctive atomic line characteristic of hydrogen atoms. Additionally, the spectral line observed at 656.3 nm is representative of the Balmer series, originating from the transition of hydrogen atoms between energy levels 3 and 2. The specific presence of the chlorine (Cl) line, notably located at 725.7 nm, serves as a distinctive indicator of the presence of PVC material (Ornik et al., 2020). The emission line at 777.3 nm denotes the transition of O(I) atoms from the $2s^22p^33s$ state to the $2s^22p^33p$ state. Ultimately, the identified spectral lines at 279.4 nm and 588.9 nm stand as distinctive indicators of Mn and Na, respectively. These findings underscore the potential of LIBS in detecting heavy metals (Zainuddin & Syuhada, 2020; Ojeda et al., 2009; Ornik et al., 2020; Araujo et al., 2018).

Table 5.1: Atomic Spectra Lines That Were Identified in The LIBS Spectra

Species (Element)	Wavelength (nm)	Electronic Transition	Reference
C	247.8	$2s^2 2p^2 - 2s^2 2p^3 s$	(Kim & Choi, 2019; Danko et al., 2013; Grégoire et al., 2011)
H	388.4	Characteristic emission line for H	(Gondal & Siddiqui, 2007; Kim & Choi, 2019)
Na	588.9	Characteristic emission line for Na	(Gondal & Siddiqui, 2007; Kim & Choi, 2019)
H	656.3	$n = 3$ to 2 (Balmer- α)	(Grégoire et al., 2011; Danko et al., 2013; Tran et al., 2001)
N	746.3	$2s^2 2p^2 3s - 2s^2 2p^2 3p$	(Grégoire et al., 2011; Kim & Choi, 2019)
Cl	725.7	Signature line for Cl	(Sattmann et al., 1998; Grégoire et al., 2011)
O(I)	777.3	$2s^2 2p^3 3s - 2s^2 2p^3 3p$	(Kim & Choi, 2019; Grégoire et al., 2011)

5.3.7 Average Number of C and H atoms and the C/H Ratios

The H and C atoms play a vital role in the collective structure of plastics. Thus, the C/H ratio can be applied in fingerprinting various polymers which make up the microplastics. P.E. was able to show a relatively higher C/H ratio; the degree of crystallinity is a determinant factor of the density of P.E., thus the high the degree of crystallinity, the high the density, and thus the C/H ratio obtained for P.E. is an indication that the microplastic particle is of HDPE polymer (Araujo et al., 2018). On the other hand, P.S. is made from a benzene ring and a substituted methyl group, and its ratio was found to be 1.40. PVC has a unique spectrum and can be easily identified due to the Cl emission line at 725.7 nm and having the least C/H ratio (Grégoire et al., 2011). The general look of the LIBS spectra for common polymers which build up the microplastics appear similar. However, their intensity ratios are different, and thus they can be distinguished (Kim & Choi, 2019). The various numbers of atoms both at 247.8nm and 388.4 nm play a critical role in calculating the C/H ratios (Gondal & Hussain, 2017). The average numbers and the C/H ratios for the detected microplastics are given in Table 5.2 as a summary.

Table 3.2: Average Number of Atoms and C/H Ratios

Polymer type	Average Number of C atoms at 247.8nm	Average Number of H atoms at 388.4nm	C/H Ratio
PET	816	736	1.11
PVC	99	111	0.89
PP	283	241	1.17
PS	531	380	1.40
PE	1122	715	1.56

5.4 Analysis of Heavy Metals

Heavy metals are a group of metals and metalloids which have toxicity even at low concentrations (Parts per billion) and also have a higher density as compared to water. These metals are also poisonous even at lower concentrations. These metals are classified into two; non-important metals such as (Zr, Ba, Li and Al), important metals include (Co, Fe, Cu, Cr and Zn), low toxicity metals such as (As and Sn) and the most toxic metals such as (Hg, Pb and Cd) (Collin et al., 2022). Presence of hard metals in our food chain has led to increased bioaccumulation in the biological tissues. Sometimes the rate of the ingestion of these metals maybe higher than the rate of excretion and this results into bioaccumulation (Khan et al., 2015).

5.4.1 Detection of Pb and Sb

Lead (Pb) is heavy metal that is created by nature and which reacts with water or air to form lead sulfate or lead oxide respectively. Existence of lead in the environment is associated to environmental processes such as mining. The allowed levels of Pb as given by the WHO are 0.01mg/l (Collin et al., 2022). This shows how toxic the element is. In five out of the 14 samples lead was detected at 280.2 nm as shown in figure 5.9. On the other hand, antimony is a heavy metal that appears in atomic number 51 on the periodic table and is majorly applied in industries for manufacture of semiconductors. Antimony is naturally existent in the earth's crust and can be liberated into air through natural discharges plastic bottled water contamination may result from industrial processes. Antimony was detected at 338.3 nm as shown in figure 5.9. According to WHO oral uptake of antimony exceeds one that comes from inhalation. The allowed guidelines for antimony are 0.1 to 0.2 2 mg/liter (Edition, 2011).

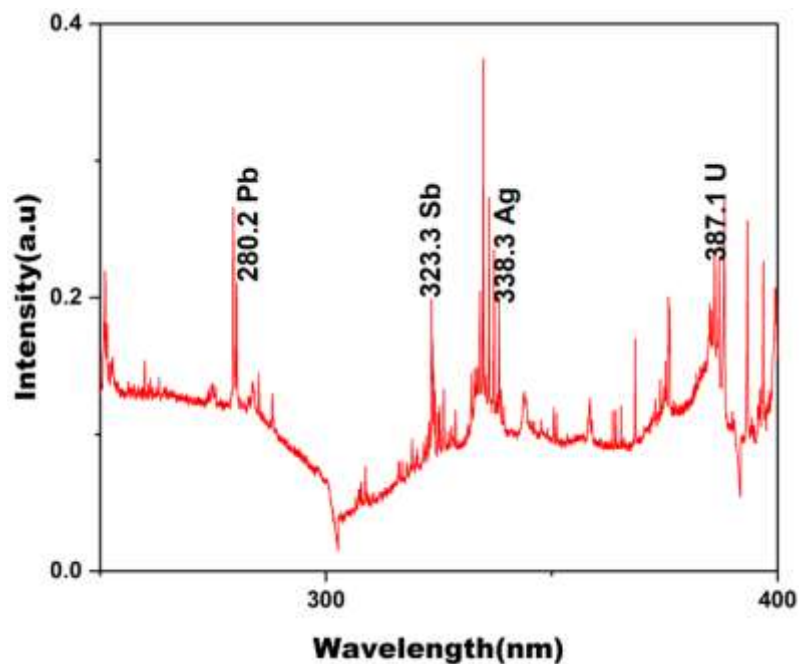


Figure 5.9: Detection Wavelengths for Pb and Sb

5.4.2 Detection of U and Hg

Uranium is a silvery grey metal that is located in the actinide series on the periodic table and it is a radioactive element. According to (Edition, 2011) low to moderate exposures to radiation may increase the incidence of cancer and genetic disorders. In this study Uranium was detected at 393.3 nm as shown in figure 5.10. Uranium contamination can result from air or during the manufacture process of the plastics. Mercury on the other hand is a hazardous element that has become widespread in the airspace due to human processes. When mercury interacts with aquatic environment it forms a more toxic compound called methylmercury (Gworek et al., 2020). The methylmercury can get into the human body by ingestion of contaminated foods and after being absorbed it can lead to various neurological problems. The guidelines given by WHO for the intake of mercury in drinking water are 0.006mg/liter (Edition, 2011). Mercury was detected at 567.8 nm as shown in figure 5.10.

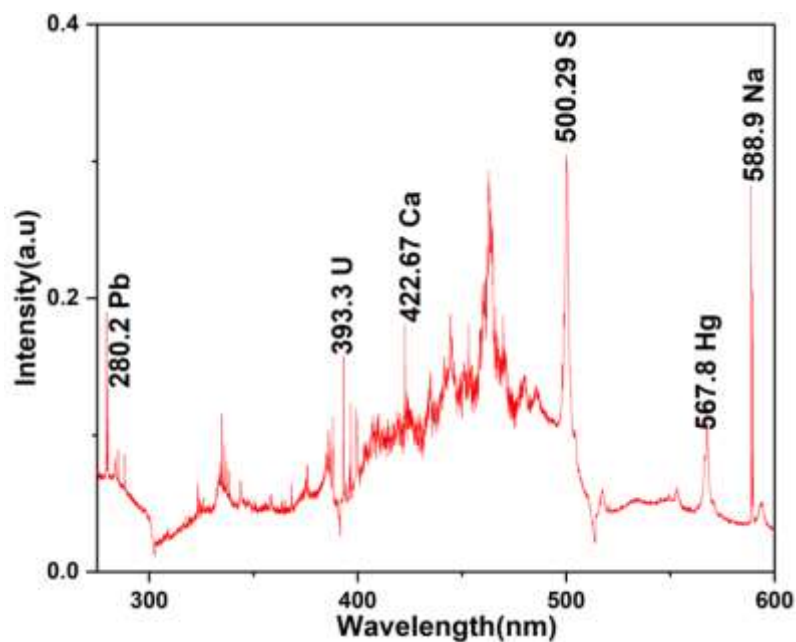


Figure 5.10: Detection Wavelengths for U and Hg

5.4.3 Detection of Mn and Na

Mercury is one of the plentiful heavy metals and is present in nature in several states of oxidation. Manganese is required for proper functioning of the body; however, excessive consumption can result to toxicity (Mitra et al., 2022). The WHO allowed guideline for manganese is 0.4 mg /liter. Manganese was detected at 279.5 nm as shown in figure 5.10. Conversely, sodium is affiliated to the alkali metals group in the periodic table. It is a silvery white metal and is the most abundant element on Earth, constituting approximately 2.8% of the Earth's crust. Na is employed as a filler in plastics, significantly enhancing their transparency. Additionally, it reinforces the plastic, leading to improved stability and excellent dispersion. This exemplifies the capability of LIBS to detect crucial trace elements. The permissible levels of sodium intake are set at 200 mg per liter, while no specific health guidelines have been established.

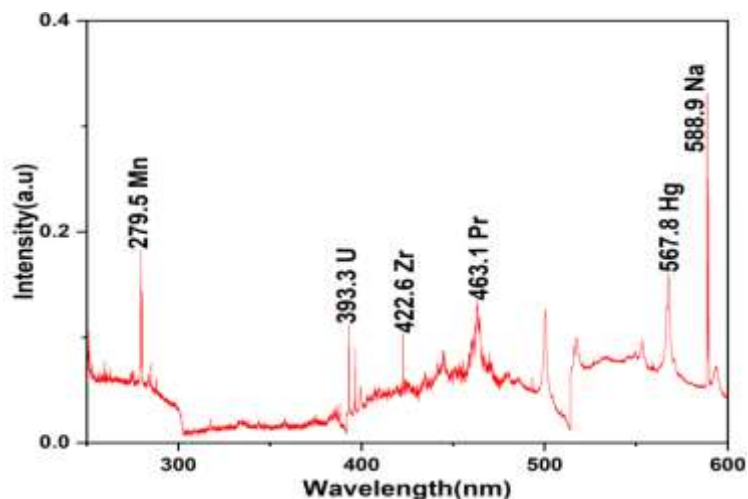


Figure 5.10: Detection Wavelengths for Mn and Na

5.4.4 Detection of Rare Earth Metals

These are a group of metals which consist of 15 elements in the lanthanide series. These metals have the same physiochemical properties and ionic radii and they are subdivided to three groups on the basis of masses and atomic number (Brouziotis et al., 2022). These subdivisions include light, middle and heavy rare earth metals. Praseodymium (Pd) which is a light rare earth metal was detected at 229.6nm as shown in figure 5.11. Rare earth metals are mostly used for the manufacture of technological devices. REEs have been shown to cause DNA damage (Brouziotis et al., 2022).

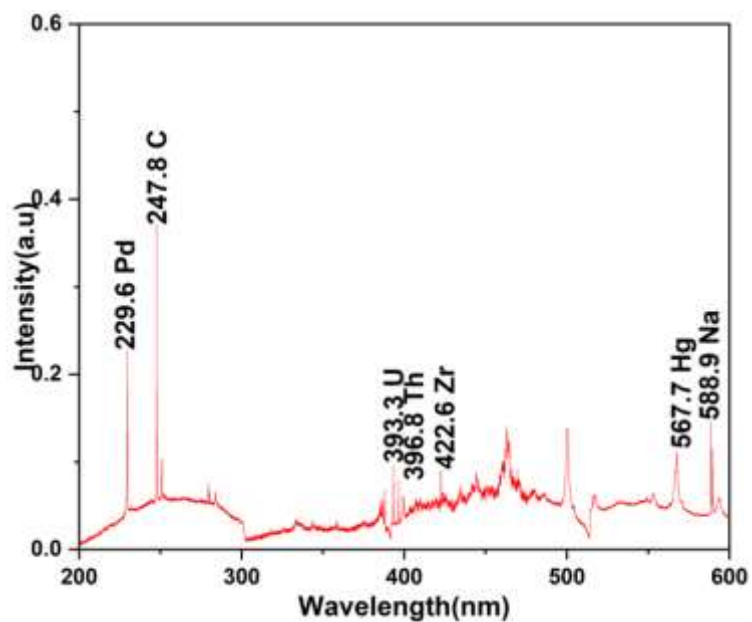


Figure 5.11: Detection Wavelengths for Rare Earth Metals

5.3.5 Possible Human Health Effects of Heavy Metals

Existence of heavy metals in the human body results to many complications which are not limited to the Alzheimer's condition, multiple sclerosis and Parkinson's disease (Neeti & Prakash, 2013). In the presence of water mercury can be converted to methyl mercury which creates sediments that are more toxic is more toxic (Rice et al., 2014). The heavy metals can also lead to physical disorders, neurological disorders, muscular effects and other acute effects which include nausea, drowsiness, vomiting, renal failure and abdominal pains (Sun et al., 2018). Human beings use these hard metals for various purposes which have greatly resulted to environmental pollution. The presence of these organic pollutants has been widely studied however the issue of heavy metals on plastics is an area of interest (Ashton et al., 2010). Surfaces of plastics are well known for the accumulation of hard metals which normally result from environmental sorption and contamination during production. Moreover, the adsorption of heavy metals to the

polymers is enhanced by the aging of the material which results to increase in surface area, porosity and polarity (Ashton et al., 2010). Plastics packaging therefore can be a possible way for the heavy metal transport in our surrounding and thus the detection and analysis is essential. Table 5.3 summarizes the possible human health threats which can be caused by ingestion of these heavy metals.

Table 5.3: Possible Impacts of Heavy Metals on The Health of Humans.

Species	Possible Source of contamination	Possible Health effects
Lead (Pb)	Human activities (mining, manufacturing, fossil fuel burning) (Loh et al., 2016)	Renal failure, interstitial fibrosis, hyperplasia, Damage to the DNA, Intellectual abnormalities in children, carcinogenic, liver damage (Hou et al., 2013; Lentini et al., 2017).
Mercury (Hg)	Sea food, human activities (Gworek et al., 2020).	Acute dyspnea, altered mental status, hypotension, tubular failure, carcinogenic, coronary heart disease (Ali et al., 2020; Crespo-López et al., 2009; Kulka, 2016).
Antimony (Sb)	Volcanic activities and weathering, anthropogenic activities (He et al., 2019).	Pancreatitis, carcinogenic, chronic bronchitis, cardiotoxicity, chronic emphysema (Sundar & Chakravarty, 2010).
Uranium (U)	Human activities (Dewar, 2019).	Renal failure, DNA damage, carcinogenic (Brugge et al., 2005).
Manganese (Mn)	During combustion of MMT (O’Neal et al., 2015)	Alteration of homeostasis and apoptotic cell death (Harischandra et al., 2019).

5.5 Raman and Laser Induced Breakdown Spectra for Polystyrene

5.5.1 Raman Spectra for Standard PS at 785 nm (250 mW and 500 mW)

The analysis of Polystyrene microplastics using 785 nm laser wavelength with laser power varied between 250 mW and 500 mW indicated no significant difference. Raman bands were observed at 336 cm^{-1} , 648 cm^{-1} , 914 cm^{-1} , 948 cm^{-1} , 1138 cm^{-1} , 1677 cm^{-1} , and 2214 cm^{-1} for both 250 mW and 500 mW as shown in figure 5.12. Theoretically the Raman signal has a direct proportionality relationship with the Raman laser power. For most cases the goal is to find a balance between laser power and sample decomposition. The laser used in this case was a continuous wave laser with laser power ranging between 1 mW- 500 Mw. High laser power is known to cause destruction to the sample as a result of burning. For this case there was no sample damage for both 250mW and 500 mW because there was no physically observed degradation, the peaks did not shift to lower frequencies and there was no large background in the obtained spectrum. Darker samples are often greatly affected by higher laser powers because their absorption bands maybe closer to the excitation wavelength. Using 250 mW and 500 mW does not cause any visible damage to the sample. In Raman spectroscopy the choice of laser power is essential due to the combination of vibrational and electronic excitations (Vandenabeele et al., 2007).

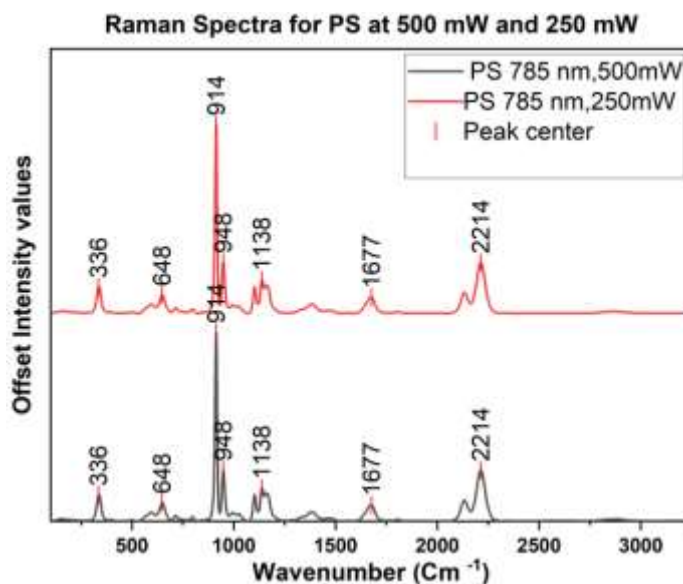


Figure 5.12: Raman spectra for Polystyrene Standard Sample Using 785 nm and Showing a Comparison Between 250 mw and 500 mW Laser Powers.

5.5.2 Raman Spectra for PS at 785 nm and 532 nm Laser Wavelengths

Raman spectrometer provides an analysis of inelastic scattered light using an interferometer or a charge coupled device. The various settings of the Raman instruments can significantly affect the quality of the Raman Spectra. Choosing the laser wavelength is one of the key considerations in the choice of a Raman spectrometer. The two most widely used wavelengths in the analysis of polymers are the near infrared 532 nm and 785 nm. However, in the examination of polymers 785 nm is the most commonly used. In the present study it was observed that for polystyrene microplastics using 532 nm produced more and intense peaks as compared to 785 nm. For 785 nm Raman bands were observed at 914 cm^{-1} , 948 cm^{-1} , and 2214 cm^{-1} . For 532 nm Raman peaks were seen at 999 cm^{-1} , 1028 cm^{-1} , 1601 cm^{-1} , 2899 cm^{-1} and 3050 cm^{-1} as indicated in figure 5.13. With the use of 532 nm two new bands were introduced at 2899 cm^{-1} and 3050 cm^{-1} . These results are in

tandem with literature because the Raman intensity has an inverse relationship with the fourth power of laser excitation wavelength (Par et al., 2019). This infers that for excellent Raman sensitivity then it's obvious that the best choice would a shorter laser wavelength and for this case 532 nm. Both laser wavelengths have their merits and demerits; 785 nm offers an excellent balance between suppression of fluorescence and the signal quality which are key determinants on the overall performance. On the other hand, 532 nm offers a better signal to noise ratio, however there is fluorescence at the expense of signal quality (Par et al., 2019). For capturing the diverse characteristics of microplastics it will be essential to combine various excitation sources.

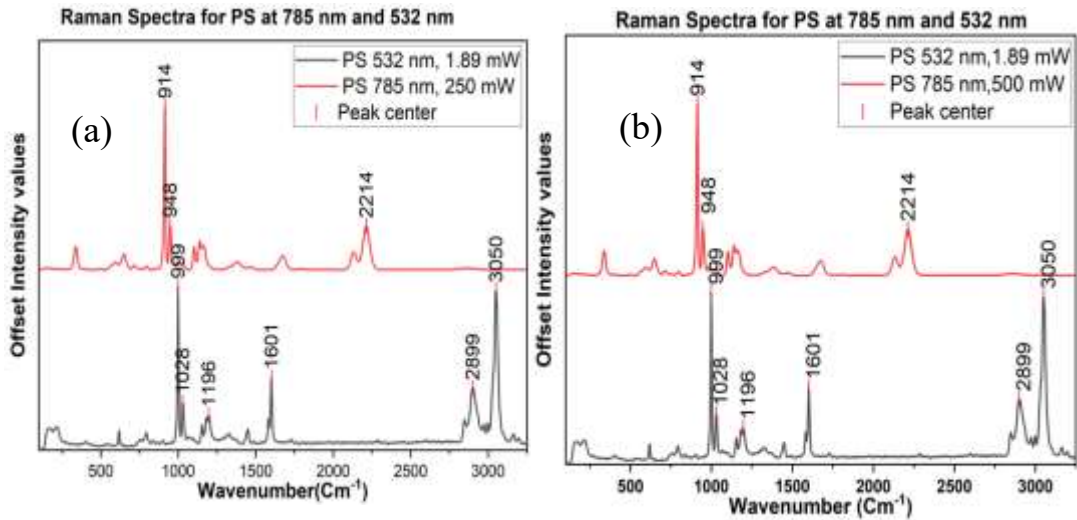


Figure 5.13: (a) Raman spectra for polystyrene standard sample using 785 nm (250mw) and 532 nm (b) Raman spectra for polystyrene standard sample using 785 nm (500mw) and 532 nm, they highlight the differences between 785 nm and 532 nm laser wavelengths.

5.5.3 Raman Band Assignments for standard PS

The Raman bands observed, as depicted in Figure 5.14, include the following wavelengths: 617 cm^{-1} , which corresponds to the deformation vibrations of the benzene ring; 999 cm^{-1} ,

arising from the aromatic carbon ring breathing mode; 1028 cm^{-1} , attributed to C-H deformation; 1196 cm^{-1} , resulting from C-C stretching vibrations; 1451 cm^{-1} , associated with CH_2 scissoring vibration; 1601 cm^{-1} , indicative of stretching of the ring skeletal and C=C bond vibrations; 2899 cm^{-1} , due to the antisymmetric vibrations of the CH_2 bond stretching mode; and 3050 cm^{-1} , originating from the C-H bond stretching within the ring (Nava et al., 2021). The vibrational frequencies are influenced by the atom masses and the strength of the bonds between them. Heavier atoms with weaker bonds tend to exhibit lower Raman shifts, while lighter atoms with stronger bonds tend to result in higher Raman shifts (Kniggendorf et al., 2019).

The C-H vibrations will tend to have a high frequency of vibration as compared to C-C vibrations for obvious reason that hydrogen has less mass compared to carbon. The C=C double bonds are stronger and hence occur at higher frequencies as compared C-C bonds which are connected by weak single bonds (Nava et al., 2021).

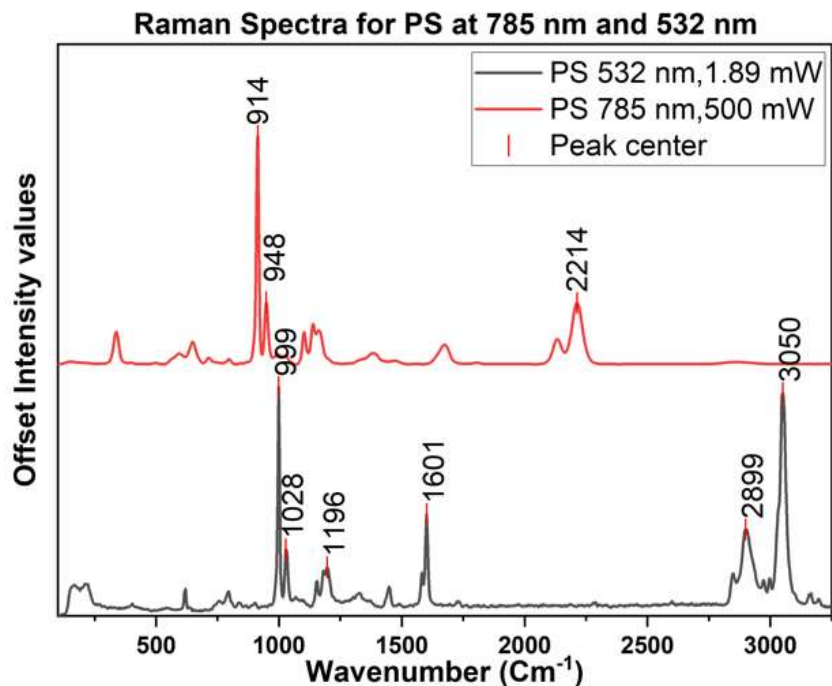


Figure 5.14: Raman spectra for PS at 785 nm and 532 nm which shows the identified Raman bands

5.5.4 Atomic Spectra for the Standard PS sample

The LIBS method is powerful in the examination of the chemical composition of various materials. The pulsed laser ablation that is generated when the surface of polystyrene is irradiated contains excited ions and atoms which are characteristic to the various elements that exist in the sample. The main elements that were observed include Carbon observed at 247.8 nm, Hydrogen observed at 656.0 nm, Sodium observed at 588.9 nm and oxygen observed at 777.3 nm as shown in figure 5.15. It can be observed that the atomic emissions are intense enough and hence cannot be affected by other emissions. Since the C and H atoms are the main components of polystyrene and hence their ratio can be used to distinguish it from other polymers. Polystyrene is an aromatic polymer; it can be

distinguished by the presence of a benzene ring which contains delocalized C-C bonds (Kim & Choi, 2019).

The structure of polystyrene comprises of the styrene monomer and does not have a heteroatom hence the presence of oxygen, nitrogen and sodium can be justified by the fact the experiment was carried out in an open environment which might have resulted to contamination from air.

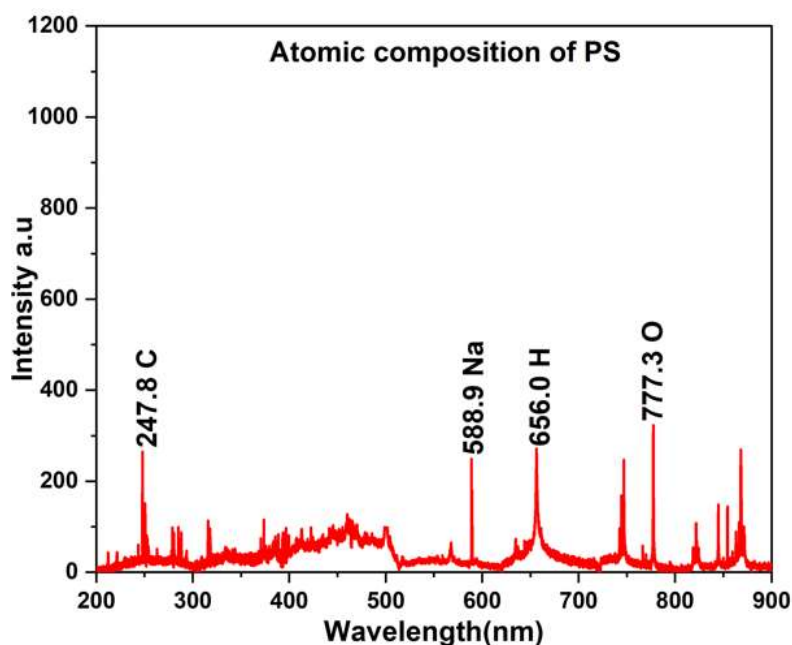


Figure 5.15: Atomic spectra for PS standard sample showing the detected elements

5.5.5 Comparison Between the Standard and the Detected PS

On comparing the Raman spectra of the standard polystyrene sample with previously obtained Raman spectra for sample 13 various differences were noted; the peaks 1002 cm^{-1} and 1032 cm^{-1} were shifted towards the left. In comparison to sample 13, the detected peaks were found to be amplified on the standard sample. Figure 5.16 illustrates that certain peak, such as 1450 cm^{-1} , 1601 cm^{-1} , 2899 cm^{-1} , and 3050 cm^{-1} , exhibited greater amplification in the standard sample. The observed shift of peaks towards lower

wavenumbers correlates with the chemical bond length of the involved molecules. Longer bond lengths result in a shift towards lower wavenumbers, whereas shorter bonds cause a shift towards higher wavenumbers. The shift towards lower wavenumbers also suggests that the sample has experienced stress. This implies that the polystyrene molecules in sample 13 may have undergone stress due to the presence of overlying polymer molecules. Additionally, it is crucial to highlight that the intensity of the Raman signal is directly proportional to the concentration of the molecules of interest. Consequently, the Raman spectra of the standard polystyrene sample exhibited higher intensity in comparison to those obtained from sample 13. For the LIBS spectra the major difference is spotted on the part of signal quality to noise ratio. LIBS spectra for sample 13 from bottled water spectra were noisier as compared to the LIBS spectra for the standard Polystyrene sample. The reason for this is that sample 13 was more contaminated as compared to the standard polystyrene and this is evident by the large number of unidentified peaks. The C/H ratio previously obtained was 1.40 whereas the one obtained from the standard Polystyrene sample was 1.18. In arriving at 1.40 the Gondal method was used which involved finding a ratio between number of atoms at 247.8 nm and 388.4 nm (Gondal & Siddiqui, 2017). For the latter the Eunok Kim method was used which involved finding a ratio between 247.8 nm and 656.3 nm (Kim & Choi, 2019). The emission line which represents a Balmer transition for Hydrogen was chosen because the peak at 388.4 nm was not intense enough and it was possibly interfered with by other emission lines. Other studies have also employed 486.8 nm for distinction of various polymers. However, the C/H ratio obtained in the present study is closer to 1.19 for polystyrene which was obtained by (Kim & Choi, 2019).

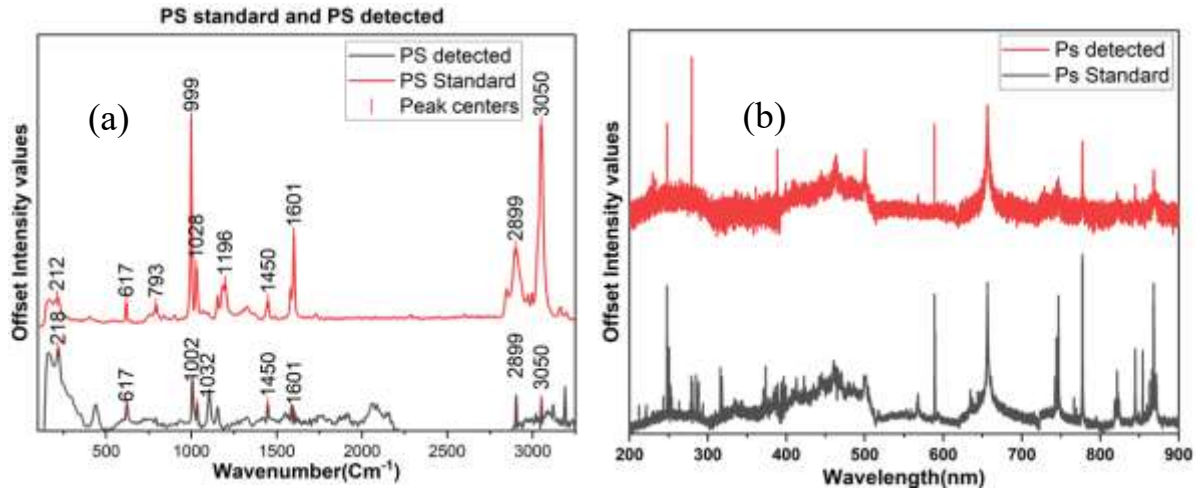


Figure 5.16: (a) Raman spectra for the standard PS in comparison with Raman spectra from the detected PS (b) LIBS spectra for the standard PS in comparison with LIBS spectra from the detected PS

5.5.6 Principal Component Analysis (PCA)

PCA findings are an indication that the large data can be visualized easily by the use of a 3D scatter plot. The 3D scatter plot captures 99.8% of the original data, this shows that most information and variance in the original data has been preserved. We used ten spectra of each 785 nm (250 mW and 500 mW) and 532 nm. The figure 5.17 demonstrates a very clear segregation between 785 nm and 532 nm which further supports the findings of this study that laser wavelength that is used for Raman spectroscopy has a significant effect on the Raman signal. Since the Raman signal intensity is inversely proportional to the fourth power of the laser wavelength, it thus follows that as the laser wavelength increases there is a decrease in the intensity of Raman scattering (Par et al., 2019). The figure 5.17 also shows unclear segregation between 250 mW and 500 mW laser powers while using 785 nm which also supports our findings that there is minimal effect of the laser power on the

Raman spectra for Polystyrene sample that was studied. The two laser powers contained similar profiles and this can be seen from the way they cluster together in the scatter plot. The reason for this might be that the laser power 250 mW and 500 mW are both optimal for the study of Polystyrene because no sample damage was observed. In using either laser powers there was a perfect balance between Raman signal intensity, the avoidance of sample damage and the minimization of interference from fluorescence. The PC1 revealed the most variation followed by PC2 and PC3. Therefore, through the use of PCA it was possible to identify the trends in the various spectra data that was obtained from Raman spectroscopy.

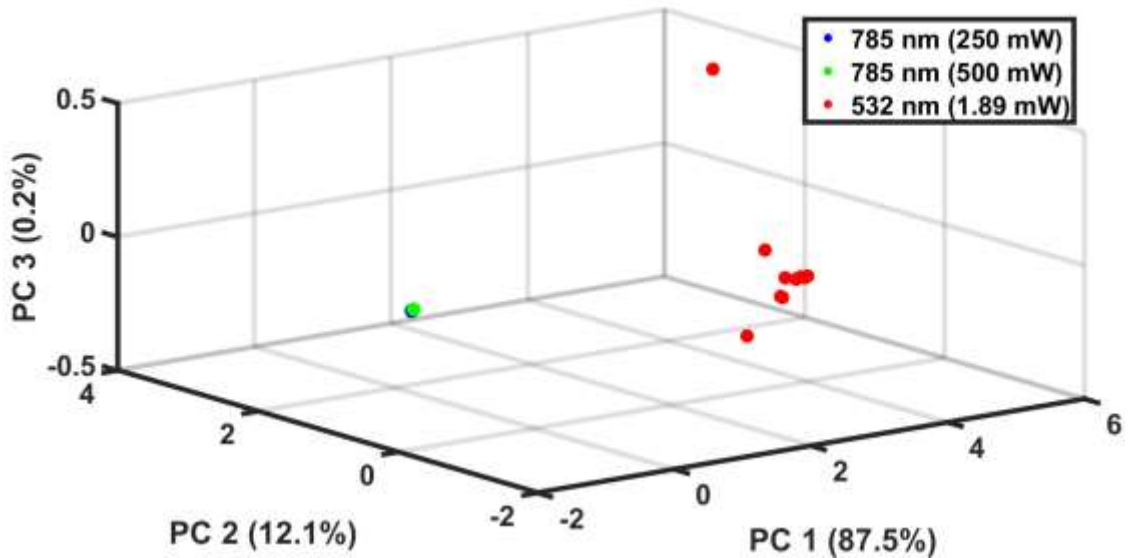


Figure 5.17: 3D Scatter Plot Showing PC Components for 785 nm and 532 nm

CHAPTER 6

CONCLUSIONS AND RECOMMENDATIONS

6.1 Conclusions

On the basis of the present work the following conclusions can be drawn;

- The microplastics found in plastic bottled drinking water are of PS, PP, PET, PVC and PE in nature. The abundances in percentage form as reported from the samples include 35.7% for Polyethylene (PE), 28.57% for Polyethylene Terephthalate (PET) 14.28% each for PP and PS. PE was the most dominant having appeared in 5 out of the 14 samples, followed by PET having appeared in 4 out of the 14 samples, PP and PS were present in 2 samples each and PVC was present in 1 sample. The reported C/H ratio from this current work for PVC (0.89), PET (1.11), PP (1.17), PS (1.40) and PE (1.56) and the trend is PE > PS > PP > PET > PVC.
- The analysis of heavy metals in the plastic packaging indicated the presence of Pb, Sb, Hg, U, Mn, Zr, Pr, and Th.
- The molecular spectra for polystyrene showed distinctive peaks at 999 cm^{-1} , 1028 cm^{-1} , 1601 cm^{-1} , 2899 cm^{-1} , and 3050 cm^{-1} .
- The atomic spectra for polystyrene provided a C/H ratio of 1.18.
- The 3D scatter plot clusters Raman spectra obtained using 250 mW and 500 mW laser powers, while segregating 532 nm from 785 nm laser wavelengths.
- On comparing sample 13 with the standard polystyrene sample, it was observed that most peaks that were in the sample were also in the standard sample which provides validation for the obtained results. For polystyrene microplastics using

250 mW and 500 mW does not have any noticeable effect on the obtained Raman Spectra.

- However, changing the laser wavelength from 785 nm to 532 nm amplifies peaks for polystyrene and introduces other new peaks in the higher frequencies. The results are supported by 3D scatter plot which clusters 250mW and 500mW but segregates 532 nm from 785 nm.
- The results obtained demonstrate that the amalgamation of Raman and LIBS methods presents a rapid and reliable alternative for the detection and identification of microplastics. They exhibit high resolution, enabling the detection of smaller particles. The utilization of these techniques in industrial settings can facilitate detecting and identifying microplastics, as well as the analysis of heavy metals, ensuring the provision of clean water and promoting responsible manufacturing practices that contribute to an improved quality of life.

6.2 Recommendations

Further research recommendations have been outlined to explore the existence of microplastics in plastic drinking water (plastic bottled) and the occurrence of heavy metals on plastic packaging. The following suggestions are provided:

- Expanding the range of spectroscopic methods for detecting, identifying, and quantifying microplastics. While this study focused on qualitative aspects, future work should aim to quantify the concentration of microplastics in specific samples. It is important to investigate whether higher concentrations of microplastics pose greater risks to human health. Additionally, exploring

multiple molecular and elemental analysis methods would enhance the comprehensiveness of the research.

- Utilizing alternative methods to quantify heavy metals in plastic packaging. While LIBS was employed in this study for heavy metal analysis, incorporating other elemental examination techniques would allow for a more comprehensive quantification of heavy metals in the identified samples.
- Obtaining additional standard samples to validate the results obtained and reduce reliance on literature. In this current study, the results were validated using a standard sample for polystyrene microplastics. To enhance the reliability of the research findings, it is recommended to obtain a broader range of standard samples for validation

REFERENCES

- Ali, S., Awan, Z., Mumtaz, S., Shakir, H. A., Ahmad, F., Ulhaq, M., & Khan, M. A. (2020). Cardiac toxicity of heavy metals (cadmium and mercury) and pharmacological intervention by vitamin C in rabbits. *Environmental Science and Pollution Research*, 27, 29266-29279.
- Andrady, A. L. (2017). The plastic in microplastics: A review. *Marine pollution bulletin*, 119(1), 12-22.
- Andreassen, E. (1999). *Infrared and Raman spectroscopy of polypropylene*. Polypropylene: an AZ reference, 320-328.
- Araujo, C. F., Nolasco, M. M., Ribeiro, A. M., & Ribeiro-Claro, P. J. (2018). Identification of microplastics using Raman spectroscopy: Latest developments and future prospects. *Water research*, 426-440.
- Ashton, K., Holmes, L., & Turner, A. (2010). Association of metals with plastic production pellets in the marine environment. *Marine pollution bulletin*, 60(11), 2050-2055.
- Baibarac, M., Stingescu, L., Stroe, M., Negri, C., Matei, E., Cotet, L. C., & Baia, L. (2021). Poly (vinyl chloride) spheres coated with graphene oxide sheets: From synthesis to optical properties and their applications as flame-retardant agents. *Polymers*, 13(4), 565.
- Blackburn, K., & Green, D. (2022) The potential effects of microplastics on human health: What is known and what is unknown, *Ambio*, vol. 51, no. 3, pp. 518-530.
- Brouziotis, A. A., Giarra, A., Libralato, G., Pagano, G., Guida, M., & Trifuoggi, M. (2022). Toxicity of rare earth elements: An overview on human health impact. *Frontiers in Environmental Science*, 10, 948041.
- Brugge, D., deLemos, J. L., & Oldmixon, B. (2005). Exposure pathways and health effects associated with chemical and radiological toxicity of natural uranium: a review. *Reviews on environmental health*, 20(3), 177-194.
- Charfi, B., & Harith, M. A. (2002). Panoramic laser-induced breakdown spectrometry of water. *Spectrochimica Acta Part B: Atomic Spectroscopy*, 57(7), 1141-1153.
- Chen, D., Wang, T., Ma, Y., Wang, G., Kong, Q., Zhang, P., & Li, R. (2020). Rapid characterization of heavy metals in single microplastics by laser induced breakdown spectroscopy. *Science of The Total Environment*, 743, 140850.
- Cheng, X., Yang, X., Zhu, Z., Guo, L., Li, X., Lu, Y., & Zeng, X. (2017). On-stream analysis of iron ore slurry using laser-induced breakdown spectroscopy. *Applied optics*, 56(33), 9144-9149.
- Collin, M. S., Venkatraman, S. K., Vijayakumar, N., Kanimozhi, V., Arbaaz, S. M., Stacey, R. S., & Swamiappan, S. (2022). Bioaccumulation of lead (Pb) and its effects on human: A review. *Journal of Hazardous Materials Advances*, 7, 100094.

- Collin, M. S., Venkatraman, S. K., Vijayakumar, N., Kanimozhi, V., Arbaaz, S. M., Stacey, R. S., & Swamiappan, S. (2022). Bioaccumulation of lead (Pb) and its effects on human: A review. *Journal of Hazardous Materials Advances*, 7, 100094.
- Costanza, R., Fioramonti, L., & Kubiszewski, I. (2016). The UN sustainable development goals and the dynamics of well-being. *Frontiers in Ecology & the Environment*, 14(2).
- Crespo-López, M. E., Macêdo, G. L., Pereira, S. I., Arrifano, G. P., Picanco-Diniz, D. L., do Nascimento, J. L. M., & Herculano, A. M. (2009). Mercury and human genotoxicity: critical considerations and possible molecular mechanisms. *Pharmacological research*, 60(4), 212-220.
- Danko, M., Orszagh, J., Ďurian, M., Kočišek, J., Daxner, M., Zöttl, S., & Matejčík, Š. (2013). Electron impact excitation of methane: determination of appearance energies for dissociation products. *Journal of Physics B: Atomic, Molecular and Optical Physics*, 46(4), 045203.
- Di, M., & Wang, J. (2018). Microplastics in surface waters and sediments of the Three Gorges Reservoir, China. *Science of the Total Environment*, 616, 1620-1627.
- Edition, F. (2011). Guidelines for drinking-water quality. *WHO chronicle*, 38(4), 104-8.
- Fischer, A. C., Kroon, J. J., Verburg, T. G., Teunissen, T., & Wolterbeek, H. T. (2007). On the relevance of iron adsorption to container materials in small-volume experiments on iron marine chemistry: 55Fe-aided assessment of capacity, affinity and kinetics. *Marine Chemistry*, 107(4), 533-546.
- Furukawa, T., Sato, H., Kita, Y., Matsukawa, K., Yamaguchi, H., Ochiai, S., & Ozaki, Y. (2006). Molecular structure, crystallinity and morphology of polyethylene/polypropylene blends studied by Raman mapping, scanning electron microscopy, wide angle X-ray diffraction, and differential scanning calorimetry. *Polymer journal*, 38(11), 1127-1136.
- Ghosal, S., Chen, M., Wagner, J., Wang, Z. M., & Wall, S. (2018). Molecular identification of polymers and anthropogenic particles extracted from oceanic water and fish stomach—A Raman micro-spectroscopy study. *Environmental Pollution*, 233, 1113-1124.
- Gondal, M. A., & Hussain, T. (2007). Determination of poisonous metals in wastewater collected from paint manufacturing plant using laser-induced breakdown spectroscopy. *Talanta*, 71(1), 73-80.
- Gondal, M. A., & Siddiqui, M. N. (2007). Identification of different kinds of plastics using laser-induced breakdown spectroscopy for waste management. *Journal of Environmental Science and Health Part A*, 42(13), 1989-1997.
- Gondal, M. A., & Siddiqui, M. N. (2007). Identification of different kinds of plastics using laser-induced breakdown spectroscopy for waste management. *Journal of Environmental Science and Health Part A*, 42(13), 1989-1997.

- Grégoire, S., Boudinet, M., Pelascini, F., Surma, F., Detalle, V., & Holl, Y. (2011). Laser-induced breakdown spectroscopy for polymer identification. *Analytical and bioanalytical chemistry*, 400, 3331-3340.
- Guo, X., Hu, G., Fan, X., & Jia, H. (2020). Sorption properties of cadmium on microplastics: the common practice experiment and a two-dimensional correlation spectroscopic study. *Ecotoxicology and Environmental Safety*, 190, 110118.
- Guo, X., Lin, Z., Wang, Y., He, Z., Wang, M., & Jin, G. (2019). In-line monitoring the degradation of polypropylene under multiple extrusions based on Raman spectroscopy. *Polymers*, 11(10), 1698.
- Gworek, B., Dmuchowski, W., & Baczewska-Dąbrowska, A. H. (2020). Mercury in the terrestrial environment: a review. *Environmental Sciences Europe*, 32(1), 128.
- Harischandra, D. S., Ghaisas, S., Zenitsky, G., Jin, H., Kanthasamy, A., Anantharam, V., & Kanthasamy, A. G. (2019). Manganese-induced neurotoxicity: new insights into the triad of protein misfolding, mitochondrial impairment, and neuroinflammation. *Frontiers in neuroscience*, 13, 654.
- He, M., Wang, N., Long, X., Zhang, C., Ma, C., Zhong, Q., & Shan, J. (2019). Antimony speciation in the environment: Recent advances in understanding the biogeochemical processes and ecological effects. *Journal of environmental sciences*, 75, 14-39.
- Holmes, L. A., Turner, A., & Thompson, R. C. (2012). Adsorption of trace metals to plastic resin pellets in the marine environment. *Environmental Pollution*, 160, 42-48.
- Hou, S., Yuan, L., Jin, P., Ding, B., Qin, N., Li, L., & Deng, Y. (2013). A clinical study of the effects of lead poisoning on the intelligence and neurobehavioral abilities of children. *Theoretical Biology and Medical Modelling*, 10, 1-9.
- Hu, J., Zuo, J., Li, J., Zhang, Y., Ai, X., Zhang, J., & Sun, D. (2022). Effects of secondary polyethylene microplastic exposure on crucian (*Carassius carassius*) growth, liver damage, and gut microbiome composition. *Science of the Total Environment*, 802, 149736.
- Hwang, J., Choi, D., Han, S., Choi, J., & Hong, J. (2019). An assessment of the toxicity of polypropylene microplastics in human derived cells. *Science of the Total Environment*, 684, 657-669.
- Kankanige, D., & Babel, S. (2020). Smaller-sized micro-plastics (MPs) contamination in single-use PET-bottled water in Thailand. *Science of the total environment*, 717, 137232.
- Khafagy, R. M. (2006). In situ FT-Raman spectroscopic study of the conformational changes occurring in isotactic polypropylene during its melting and crystallization processes. *Journal of Polymer Science Part B: Polymer Physics*, 44(15), 2173-2182.

- Khan, A., Khan, S., Khan, M. A., Qamar, Z., & Waqas, M. (2015). The uptake and bioaccumulation of heavy metals by food plants, their effects on plants nutrients, and associated health risk: a review. *Environmental science and pollution research*, 22, 13772-13799.
- Kim, E., & Choi, W. Z. (2019). Real-time identification of plastics by types using laser-induced breakdown spectroscopy. *Journal of Material Cycles and Waste Management*, 21, 176-180.
- Kim, E., & Choi, W. Z. (2019). Real-time identification of plastics by types using laser-induced breakdown spectroscopy. *Journal of Material Cycles and Waste Management*, 21, 176-180.
- Kirstein, I. V., Gomiero, A., & Vollertsen, J. (2021). Microplastic pollution in drinking water. *Current Opinion in Toxicology*, 28, 70-75.
- Kniggendorf, A. K., Wetzel, C., & Roth, B. (2019). Microplastics detection in streaming tap water with Raman spectroscopy. *Sensors*, 19(8), 1839.
- Kosuth, M., Mason, S. A., & Wattenberg, E. V. (2018). Anthropogenic contamination of tap water, beer, and sea salt. *PloS one*, 13(4), e0194970.
- Kulka, M. (2016). A review of paraoxonase 1 properties and diagnostic applications. *Polish journal of veterinary sciences*.
- Lambert, S., & Wagner, M. (2016). Characterisation of nanoplastics during the degradation of polystyrene. *Chemosphere*, 145, 265-268.
- Lazic, V., & Jovičević, S. (2014). Laser induced breakdown spectroscopy inside liquids: processes and analytical aspects. *Spectrochimica Acta Part B: Atomic Spectroscopy*, 101, 288-311.
- Lazic, V., Fantoni, R., Palucci, A., & Ciaffi, M. (2017). Sample preparation for repeated measurements on a single liquid droplet using laser-induced breakdown spectroscopy. *Applied Spectroscopy*, 71(4), 670-677.
- Lei, L., Liu, M., Song, Y., Lu, S., Hu, J., Cao, C., & He, D. (2018). Polystyrene (nano) microplastics cause size-dependent neurotoxicity, oxidative damage and other adverse effects in *Caenorhabditis elegans*. *Environmental Science: Nano*, 5(8), 2009-2020.
- Leng, Y. (2013). *Materials characterization: introduction to microscopic and spectroscopic methods*. John Wiley & Sons.
- Lentini, P., Zanolli, L., Granata, A., Signorelli, S. S., Castellino, P., & Dellaquila, R. (2017). Kidney and heavy metals-The role of environmental exposure. *Molecular medicine reports*, 15(5), 3413-3419.
- Lithner, D., Larsson, Å., & Dave, G. (2011). Environmental and health hazard ranking and assessment of plastic polymers based on chemical composition. *Science of the total environment*, 409(18), 3309-3324.

- Liu, S., Shi, J., Wang, J., Dai, Y., Li, H., Li, J., & Zhang, P. (2021). Interactions between microplastics and heavy metals in aquatic environments: a review. *Frontiers in microbiology*, 12, 652520.
- Loh, N., Loh, H. P., Wang, L. K., & Wang, M. H. S. (2016). Health effects and control of toxic lead in the environment. *Natural Resources and Control Processes*, 233-284.
- Lohumi, S., Kim, M. S., Qin, J., & Cho, B. K. (2017). Raman imaging from microscopy to macroscopy: quality and safety control of biological materials. *TrAC Trends in Analytical Chemistry*, 93, 183-198.
- Ludwig, V., Ludwig, Z. M. D. C., Rodrigues, M. M., Anjos, V., Costa, C. B., das Dores, D. R. S. A., & Soares, F. (2018). Analysis by Raman and infrared spectroscopy combined with theoretical studies on the identification of plasticizer in PVC films. *Vibrational Spectroscopy*, 98, 134-138.
- Mason, S. A., Welch, V. G., & Neratko, J. (2018). Synthetic polymer contamination in bottled water. *Frontiers in chemistry*, 6, 389699.
- Mazilu, M., Luca, A. C. D., Riches, A., Herrington, C. S., & Dholakia, K. (2010). Optimal algorithm for fluorescence suppression of modulated Raman spectroscopy. *Optics express*, 18(11), 11382-11395.
- McCreery, R. L. (2005). *Raman spectroscopy for chemical analysis*. John Wiley & Sons.
- Gardiner, D. J. (1989). Introduction to Raman scattering. In *Practical Raman Spectroscopy* (pp. 1-12). Berlin, Heidelberg: Springer Berlin Heidelberg.
- Mintenig, S. M., Löder, M. G., Primpke, S., & Gerdt, G. (2019). Low numbers of microplastics detected in drinking water from ground water sources. *Science of the total environment*, 648, 631-635.
- Mishra, S. P., Sarkar, U., Taraphder, S., Datta, S., Swain, D., Saikhom, R., & Laishram, M. (2017). Multivariate statistical data analysis-principal component analysis (PCA). *International Journal of Livestock Research*, 7(5), 60-78.
- Mitra, S., Chakraborty, A. J., Tareq, A. M., Emran, T. B., Nainu, F., Khusro, A., & Simal-Gandara, J. (2022). Impact of heavy metals on the environment and human health: Novel therapeutic insights to counter the toxicity. *Journal of King Saud University-Science*, 34(3), 101865.
- Nava, V., Frezzotti, M. L., & Leoni, B. (2021). Raman spectroscopy for the analysis of microplastics in aquatic systems. *Applied Spectroscopy*, 75(11), 1341-1357.
- Neeti, K., & Prakash, T. (2013). Effects of heavy metal poisoning during pregnancy. *Int Res J Environ Sci*, 2(1), 88-92.
- Novotný, J., Novotný, K., Prochazka, D., Hrdlicka, A., & Kaiser, J. (2014). Two dimensional elemental mapping by laser-induced breakdown spectroscopy. *Spectrosc. Eur*, 26(6), 6-10.

- O'Neal, S. L., & Zheng, W. (2015). Manganese toxicity upon overexposure: a decade in review. *Current environmental health reports*, 2, 315-328.
- Ojeda, J. J., Romero-Gonzalez, M. E., & Banwart, S. A. (2009). Analysis of bacteria on steel surfaces using reflectance micro-Fourier transform infrared spectroscopy. *Analytical Chemistry*, 81(15), 6467-6473.
- Ondieki, M. A. (2020). Raman Spectrometric Study of Influence of Acetaminophen on Female Mices Reproductive Hormone Levels Blood (Doctoral dissertation, University of Nairobi).
- Oreborn, U. (2018). IR spectroscopy for vibrational modes: A semi-classical approach based on classical electrodynamics and modern quantum mechanics.
- Ornik, J., Sommer, S., Gies, S., Weber, M., Lott, C., Balzer, J. C., & Koch, M. (2020). Could photoluminescence spectroscopy be an alternative technique for the detection of microplastics? First experiments using a 405 nm laser for excitation. *Applied Physics B*, 126, 1-7.
- Oßmann, B. E., Sarau, G., Holtmannspötter, H., Pischetsrieder, M., Christiansen, S. H., & Dicke, W. (2018). Small-sized microplastics and pigmented particles in bottled mineral water. *Water research*, 141, 307-316.
- Par, M., Gamulin, O., Spanovic, N., Bjelovucic, R., & Tarle, Z. (2019). The effect of excitation laser power in Raman spectroscopic measurements of the degree of conversion of resin composites. *Dental materials*, 35(9), 1227-1237.
- Potcoava, M. C., Futia, G. L., Aughenbaugh, J., Schlaepfer, I. R., & Gibson, E. A. (2014). Raman and coherent anti-Stokes Raman scattering microscopy studies of changes in lipid content and composition in hormone-treated breast and prostate cancer cells. *Journal of Biomedical Optics*, 19(11), 111605-111605.
- Prunier, J., Maurice, L., Perez, E., Gigault, J., Wickmann, A. C. P., Davranche, M., & Ter Halle, A. (2019). Trace metals in polyethylene debris from the North Atlantic subtropical gyre. *Environmental Pollution*, 245, 371-379.
- Qian, N. (2018). Bottled water or tap water? A comparative study of drinking water choices on university campuses. *Water*, 10(1), 59.
- Ragusa, A., Svelato, A., Santacroce, C., Catalano, P., Notarstefano, V., Carnevali, O., & Giorgini, E. (2021). Plasticenta: First evidence of microplastics in human placenta. *Environment international*, 146, 106274.
- Raja, P., & Barron, A. R. (2019). Physical methods in chemistry and nano science.
- Rebollar, E., Pérez, S., Hernández, M., Domingo, C., Martín, M., Ezquerra, T. A., & Castillejo, M. (2014). Physicochemical modifications accompanying UV laser induced surface structures on poly (ethylene terephthalate) and their effect on adhesion of mesenchymal cells. *Physical Chemistry Chemical Physics*, 16(33), 17551-17559.

- Rice, K. M., Walker Jr, E. M., Wu, M., Gillette, C., & Blough, E. R. (2014). Environmental mercury and its toxic effects. *Journal of preventive medicine and public health*, 47(2), 74.
- Rios, L. M., Jones, P. R., Moore, C., & Narayan, U. V. (2010). Quantitation of persistent organic pollutants adsorbed on plastic debris from the Northern Pacific Gyre's "eastern garbage patch". *Journal of Environmental Monitoring*, 12(12), 2226-2236.
- Rochman, C. M., Hentschel, B. T., & Teh, S. J. (2014). Long-term sorption of metals is similar among plastic types: implications for plastic debris in aquatic environments. *PloS one*, 9(1), e85433.
- Rochman, C. M., Hentschel, B. T., & Teh, S. J. (2014). Long-term sorption of metals is similar among plastic types: implications for plastic debris in aquatic environments. *PloS one*, 9(1), e85433.
- Rouillon, C., Bussiere, P. O., Desnoux, E., Collin, S., Vial, C., Therias, S., & Gardette, J. L. (2016). Is carbonyl index a quantitative probe to monitor polypropylene photodegradation?. *Polymer degradation and stability*, 128, 200-208.
- Ruas, A., Matsumoto, A., Ohba, H., Akaoka, K., & Wakaida, I. (2017). Application of laser-induced breakdown spectroscopy to zirconium in aqueous solution. *Spectrochimica Acta Part B: Atomic Spectroscopy*, 131, 99-106.
- Sattmann, R., Monch, I., Krause, H., Noll, R., Couris, S., Hatziapostolou, A., & Miguel, R. (1998). Laser-induced breakdown spectroscopy for polymer identification. *Applied Spectroscopy*, 52(3), 456-461.
- Saylor, A., Prokopy, L. S., & Amberg, S. (2011). What's wrong with the tap? Examining perceptions of tap water and bottled water at Purdue University. *Environmental management*, 48, 588-601.
- Schwabl, P., Köppel, S., Königshofer, P., Bucsics, T., Trauner, M., Reiberger, T., & Liebmann, B. (2019). Detection of various microplastics in human stool: a prospective case series. *Annals of internal medicine*, 171(7), 453-457.
- Schwarz, A. E., Ligthart, T. N., Boukris, E., & Van Harmelen, T. (2019). Sources, transport, and accumulation of different types of plastic litter in aquatic environments: a review study. *Marine pollution bulletin*, 143, 92-100.
- Schymanski, D., Goldbeck, C., Humpf, H. U., & Fürst, P. (2018). Analysis of microplastics in water by micro-Raman spectroscopy: Release of plastic particles from different packaging into mineral water. *Water research*, 129, 154-162.
- Shameem, K. M., Choudhari, K. S., Bankapur, A., Kulkarni, S. D., Unnikrishnan, V. K., George, S. D., & Santhosh, C. (2017). A hybrid LIBS–Raman system combined with chemometrics: an efficient tool for plastic identification and sorting. *Analytical and bioanalytical chemistry*, 409, 3299-3308.
- Shen, J., Liang, B., Zhang, D., Li, Y., Tang, H., Zhong, L., & Xu, Y. (2021). Effects of PET microplastics on the physiology of *Drosophila*. *Chemosphere*, 283, 131289.

- Siebert, F., Hildebrandt, P. (2008). *Vibrational Spectroscopy in Life Science*. Wiley-VCH Verlag GmbH & Co. KGaA.
- Sommer, C., Schneider, L. M., Nguyen, J., Prume, J. A., Lautze, K., & Koch, M. (2021). Identifying microplastic litter with Laser Induced Breakdown Spectroscopy: A first approach. *Marine Pollution Bulletin*, 171, 112789
- Sun, Z., Xie, X., Wang, P., Hu, Y., & Cheng, H. (2018). Heavy metal pollution caused by small-scale metal ore mining activities: A case study from a polymetallic mine in South China. *Science of the Total Environment*, 639, 217-227.
- Sundar, S., & Chakravarty, J. (2010). Antimony toxicity. *International journal of environmental research and public health*, 7(12), 4267-4277.
- Teuten, E. L., Saquing, J. M., Knappe, D. R., Barlaz, M. A., Jonsson, S., Björn, A., & Takada, H. (2009). Transport and release of chemicals from plastics to the environment and to wildlife. *Philosophical transactions of the royal society B: biological sciences*, 364(1526), 2027-2045.
- Thakur, S. N., & Singh, J. P. (2020). Fundamentals of LIBS and recent developments. *Laser-Induced Breakdown Spectroscopy*, 3-22.
- Tirkey, A., & Upadhyay, L. S. B. (2021). Microplastics: An overview on separation, identification and characterization of microplastics. *Marine pollution bulletin*, 170, 112604.
- Torres, F. G., Dioses-Salinas, D. C., Pizarro-Ortega, C. I., & De-la-Torre, G. E. (2021). Sorption of chemical contaminants on degradable and non-degradable microplastics: Recent progress and research trends. *Science of the Total Environment*, 757, 143875.
- Tran, M., Sun, Q., Smith, B. W., & Winefordner, J. D. (2001). Determination of C: H: O: N ratios in solid organic compounds by laser-induced plasma spectroscopy. *Journal of Analytical Atomic Spectrometry*, 16(6), 628-632.
- Turner, A., Wallerstein, C., & Arnold, R. (2019). Identification, origin and characteristics of bio-bead microplastics from beaches in western Europe. *Science of The Total Environment*, 664, 938-947.
- Unnikrishnan, V. K., Choudhari, K. S., Kulkarni, S. D., Nayak, R., Kartha, V. B., & Santhosh, C. (2013). Analytical predictive capabilities of laser induced breakdown spectroscopy (LIBS) with principal component analysis (PCA) for plastic classification. *Rsc Advances*, 3(48), 25872-25880.
- Vandenabeele, P., Edwards, H. G., & Moens, L. (2007). A decade of Raman spectroscopy in art and archaeology. *Chemical reviews*, 107(3), 675-686.
- Vedolin, M. C., Teophilo, C. Y. S., Turra, A., & Figueira, R. C. L. (2018). Spatial variability in the concentrations of metals in beached microplastics. *Marine pollution bulletin*, 129(2), 487-493.

- Winkler, A., Santo, N., Ortenzi, M. A., Bolzoni, E., Bacchetta, R., & Tremolada, P. (2019). Does mechanical stress cause microplastic release from plastic water bottles? *Water research*, 166, 115082.
- Wright, S. L., Thompson, R. C., & Galloway, T. S. (2013). The physical impacts of microplastics on marine organisms: a review. *Environmental pollution*, 178, 483-492.
- Yueh, F. Y., Sharma, R. C., Singh, J. P., Zhang, H., & Spencer, W. A. (2002). Evaluation of the potential of laser-induced breakdown spectroscopy for detection of trace element in liquid. *Journal of the Air & Waste Management Association*, 52(11), 1307-1315.
- Zainuddin, Z., & Syuhada. (2020, June). Study of analysis method on microplastic identification in bottled drinking water. *In Macromolecular Symposia* (Vol. 391, No. 1, p. 1900195)
- Zhang, D. C., Hu, Z. Q., Su, Y. B., Hai, B., Zhu, X. L., Zhu, J. F., & Ma, X. (2018). Simple method for liquid analysis by laser-induced breakdown spectroscopy (LIBS). *Optics express*, 26(14), 18794-18802.
- Zhao, Y., Qin, Z., Huang, Z., Bao, Z., Luo, T., & Jin, Y. (2021). Effects of polyethylene microplastics on the microbiome and metabolism in larval zebrafish. *Environmental Pollution*, 282, 117039.

APPENDICES

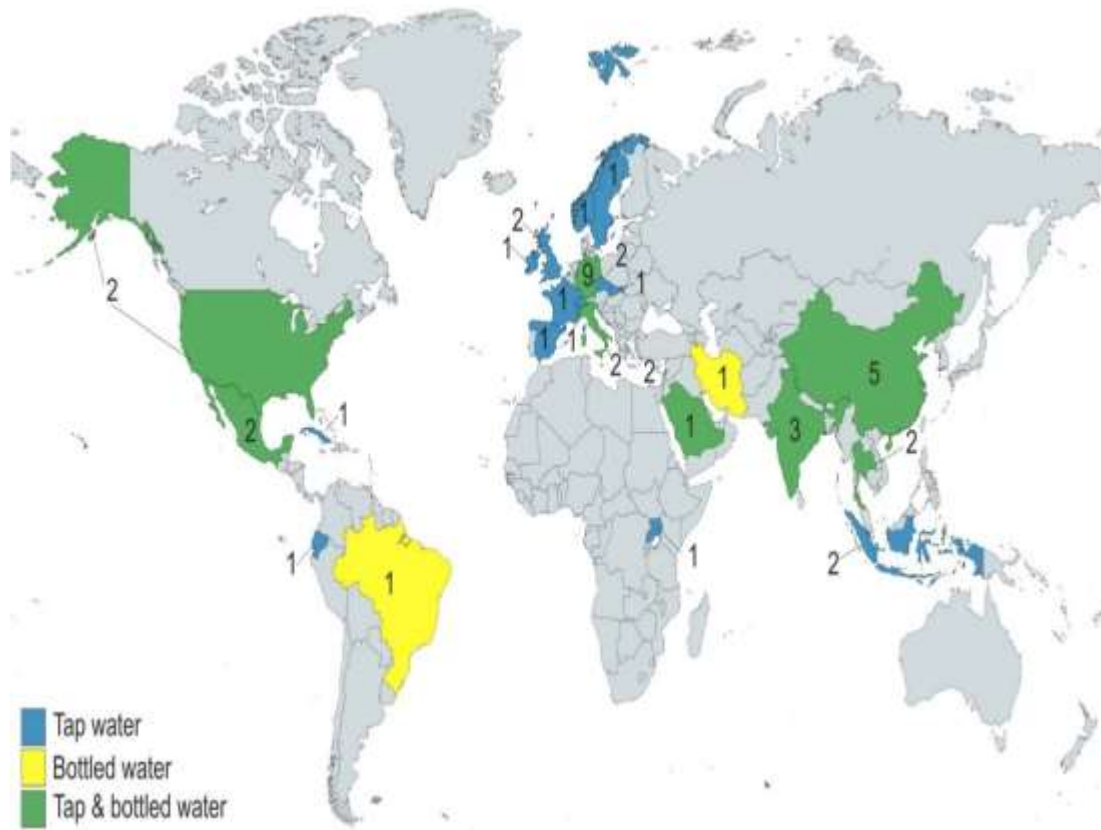


Figure 6.1: Recent microplastic studies in tap and bottled drinking water (Kirstein et al., 2021)